How selective severing by katanin promotes order in the plant cortical microtubule array

Eva E. Deinum[a,b,1], Simon H. Tindemans[b,2], Jelmer J. Lindeboom[c], and Bela M. Mulder[b,d]

[a]Mathematical and Statistical Methods, Wageningen University & Research, 6708 PB Wageningen, The Netherlands; [b]Systems Biophysics, AMOLF, 1098 XG Amsterdam, The Netherlands; [c]Department of Plant Biology, Carnegie Institution for Science, Stanford, CA 94305; and [d]Laboratory of Cell Biology, Wageningen University & Research, 6708 PB Wageningen, The Netherlands

Edited by Olivier Hamant, École Normale Supérieure de Lyon, Lyon, France, and accepted by Editorial Board Member Caroline Dean May 9, 2017 (received for review February 24, 2017)

Plant morphogenesis requires differential and often asymmetric growth. A key role in controlling anisotropic expansion of individual cells is played by the cortical microtubule array. Although highly organized, the array can nevertheless rapidly change in response to internal and external cues. Experiments have identified the microtubule-severing enzyme katanin as a central player in controlling the organizational state of the array. Katanin action is required both for normal alignment and the adaptation of array orientation to mechanical, environmental, and developmental stimuli. How katanin fulfills its controlling role, however, remains poorly understood. On the one hand, from a theoretical perspective, array ordering depends on the "weeding out" of discordant microtubules through frequent catastrophe-inducing collisions among microtubules. Severing would reduce average microtubule length and lifetime, and consequently weaken the driving force for alignment. On the other hand, it has been suggested that selective severing at microtubule crossovers could facilitate the removal of discordant microtubules. Here we show that this apparent conflict can be resolved by systematically dissecting the role of all of the relevant interactions in silico. This procedure allows the identification of the sufficient and necessary conditions for katanin to promote array alignment, stresses the critical importance of the experimentally observed selective severing of the "crossing" microtubule at crossovers, and reveals a hitherto not appreciated role for microtubule bundling. We show how understanding the underlying mechanism can aid with interpreting experimental results and designing future experiments.

katanin | cortical microtubule array | microtubule dynamics | self-organization | plant cell biology

Plant cells are constrained by their cellulose-based cell walls. This fact poses two important requirements for development: (*i*) consistent cell wall anisotropy within tissues to ensure coherent growth and (*ii*) precise local controllability of cell wall properties to produce complex cell shapes (e.g., ref. 1) and accommodate the development of new plant organs (e.g., ref. 2). The central organizing system that mediates these requirements is the plant cortical microtubule (MT) array. Individual MTs self-organize into this often strikingly ordered structure, which is known to regulate the insertion of cellulose synthase complexes into the plasma membrane (3) and subsequently guide their movement during cellulose microfibril deposition (4), thereby playing a key role in cell growth and development. The organizational state of the array, in turn, depends on cell type (5) and may change in response to mechanical (6), environmental stimuli, and developmental patterning processes (7). Acentrosomal and cortical MT arrays also occur in other eukaryotic systems, including protists and animals (e.g., refs. 8–10).

The core mechanism behind the self-organization of the array is described by a consensus model that has been developed over the past few years. Cortical MTs are attached to the plasma membrane, where they interact with each other through collisions. A single MT can undergo multiple interactions during its lifetime due to the dynamic instability of individual MTs (11), i.e., the stochastic switching between growing and shrinking phases. These switching events are called catastrophes and rescues.

When a growing cortical MT impinges on an obstructing MT, the outcome of this collision depends strongly on the angle θ between the two MTs. After shallow-angle encounters, with $\theta \lesssim 40°$, the growing MT will typically bend and continue its way along the obstructing MT, a process we refer to as "bundling" (elsewhere also referred to as entrainment or zippering) (12, 13). For larger-angle encounters, the impinging MT may either cross over the obstructing one and continue growth in its original direction, or, after a short pause, switch to a shrinking state (13), which is called an "induced catastrophe."

These interactions are sufficient to create spontaneous collective alignment of cortical MTs, as shown by both computer simulations (14–16) and analytical models (17, 18). The causative mechanism at play has been called "survival of the aligned" (17). Induced catastrophes suffered by "discordant" MTs can significantly shorten their lifetime in comparison with a majority of concordant (aligned) MTs, which have few collisions among themselves. With a sufficient number of collisions per average MT lifetime, small biases in an initially isotropic state will be reinforced, resulting in the spontaneous appearance of a majority of aligned MTs that are longer-lived and therefore attain longer average lengths.

A number of recent results point to a key role for the MT-severing protein katanin (19–22) in setting up alignment of the

Significance

The plant cortical microtubule array is a dynamic self-organizing structure that controls the mechanics of plant growth by guiding the deposition of wall material, and is required for asymmetric cell growth, the basis for plant morphogenesis. The array is acentrosomal, i.e., its self-organization is a distributed process. Acentrosomal microtubule arrays are also present in animals, e.g., in the basal cortex of polarized epithelial cells and fertilized *Xenopus* eggs. Microtubule-severing enzyme katanin is essential for normal array organization and its response to internal and external stimuli. Here, we formally identify the requirements for microtubule ordering through katanin action, including one previously unknown. This understanding provides access to the adaptive control of cell wall structure and plant growth and development.

Author contributions: E.E.D., S.H.T., J.J.L., and B.M.M. designed research; E.E.D. performed research; E.E.D. analyzed data; E.E.D., S.H.T., J.J.L., and B.M.M. wrote the paper; and E.E.D. and S.H.T. developed software.

The authors declare no conflict of interest.

This article is a PNAS Direct Submission. O.H. is a guest editor invited by the Editorial Board.

Freely available online through the PNAS open access option.

[1]To whom correspondence should be addressed. Email: eva.deinum@wur.nl.

[2]Present address: Department of Electrical and Electronic Engineering, Imperial College London, London SW7 2AZ, United Kingdom.

This article contains supporting information online at www.pnas.org/lookup/suppl/doi:10.1073/pnas.1702650114/-/DCSupplemental.

cortical array (23, 24) as well as its reorientation upon external cues (25, 26). At first sight, these findings seem at odds with the survival-of-the-aligned mechanism. It has been reported that, after severing, the newly formed plus end of the lagging MT typically starts in the shrinking state (27, 28). Previous theoretical work on noninteracting MTs has shown that, under this condition, severing uniformly along the full length of MTs does not affect the total number of MTs but does reduce average MT length (29). These shorter MTs would have fewer interactions per average MT lifetime and, consequently, a reduced potential for alignment.

Experiments suggest, however, that katanin actually promotes alignment. Loss-of-function mutations of the katanin p60 subunit result in reduced MT alignment in a range of cell types. The cells in these mutants tend to be more bulged, and the plants exhibit an overall dwarfed phenotype (20, 22). Ref. 19 also reported delayed MT alignment. Additionally, overexpression of RIC1, a protein that stimulates katanin activity, results in highly aligned arrays in pavement cells, which normally do not have aligned arrays (30).

Interestingly, in plants, MT severing appears to preferentially occur at crossover sites (31), and it has recently been shown that this requires the activity of katanin (26, 24, 32). Strikingly, these recent experimental observations also show that it is the "crossing" MT which is preferentially severed (26, 24), rather than the "crossed-over" one.

Here we dissect the influence of MT severing on the alignment process of the cortical array using both computer simulations and theoretical arguments. In the simulations, we systematically address the roles of crossover-specific versus random severing, the significance of severing only the crossing MT at crossovers, and the importance of bundling following shallow-angle encounters. Our results show that katanin-mediated severing can indeed promote array alignment, but only when severing is more likely for the crossing MT and the probability of severing at shallow-angle crossovers is low. Our work uncovers an additional requirement for severing-mediated alignment of the cortical array: a previously unknown role for MT bundling. These insights lead to the understanding of mechanisms by which tuning MT severing can be used to control the organizational state of the array.

Results

Key Aspects of the Modeling Framework. We model cortical MTs as series of connected line segments, where one free end, the plus end, exhibits dynamic instability, and the other free end, the minus end, shows steady depolymerization ("treadmilling"), characterized by parameters (*SI Appendix*, Table S1) that are based on experimental observations (16). MT collisions with relative angles $\theta \leq \theta^* = 40^\circ$ result in bundling. Collisions at larger angles result in either an induced catastrophe (with probability P_{cat}) or a crossover (Fig. 1*A*). As default, we used $P_{cat} = 0.5$ (16, 33, 34). In between collisions, MTs grow in straight lines.

In our simulations, we characterize the strength of the interactions between the MTs using a control parameter G_c. This parameter, originally derived from a theoretical model (*Materials and Methods*), combines all dynamic instability parameters and the nucleation rate in a single dimensionless number. Generically, alignment occurs when the control parameter G_c exceeds a critical value G^* (*Materials and Methods*). In most biologically relevant cases, $G_c < 0$, and its value can be interpreted as (minus) the ratio of the typical length scale between interactions and the average MT length in the absence of interactions. This interpretation intuitively suggests ways in which alignment can be enhanced by making G_c less negative (see also Table 1). The control parameter has proven very useful in investigating the effects of various processes on MT alignment, even outside the scope in which it was derived (16, 33, 35).

To quantify the degree of alignment of our simulated cortical arrays, we use the order parameter S_2, originally formulated to measure the degree of alignment in liquid crystals (*Materials and Methods*). S_2 takes values between 0, for a perfectly isotropic (disordered) system, and 1, for a system in which all MTs are aligned exactly parallel or antiparallel.

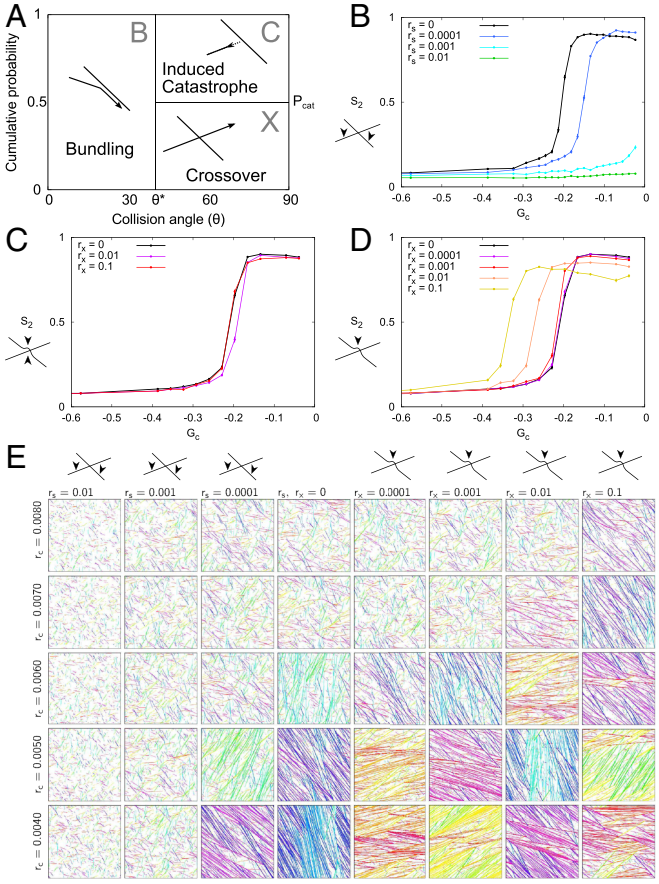

Fig. 1. Location of severing determines its effect on alignment. (*A*) Angle-dependent collision outcomes. Bundling ("B") occurs for collision angles $\theta < \theta^* = 40^\circ$; for larger angles, induced catastrophes ("C") occur with probability P_{cat}, and, otherwise, MTs cross over ("X"). (*B–D*) Alignment (S_2) as a function of G_c. (*B*) Random severing (rates per micrometer per second as indicated). (*C* and *D*) Crossover severing (rates per crossover per second as indicated) for (*C*) aselective (either side of crossover) and (*D*) crossing only. In *B–D*, error bars show the SEM, with $n = 100$ independent simulations per data point. (*E*) Representative snapshots (*SI Appendix, Unbiased Selection of Snapshots*) for various induced catastrophe rates r_c and severing rates (r_s and r_x) at $T = 30$ h. MTs are colored according to their orientation, to enhance the visibility of domains with different orientations.

By measuring the order parameter S_2 for a range of values of the control parameter G_c, we can compare, in a straightforward manner, how phenomena that are not part of G_c, such as severing, influence the system's potential for alignment (e.g., see ref. 35). Using this framework, we investigated several modes of MT severing.

Localization and Selectivity of Severing Determines Effect on Alignment.

Random severing reduces the potential to align. We first tested the theory-based (29) prediction that random severing would reduce the potential to align also in the full interacting system. For this analysis, we introduced a uniform severing rate per unit of MT length r_s (in micrometers per second) in our simulations. Increasing r_s reduced the regime of control parameter values (G_c) for which the system can align, to the point that alignment became impossible with the highest reported severing rates (Fig. 1 *B* and *E*). Moreover, in line with the theoretical predictions for the noninteracting MTs (29), we found that the MT length distributions were no longer exponential, as without severing (refs. 18

Table 1. Impact of changes in MT dynamics

	Primary effect		G_c compensated*		
Change	G_c	Possible switch	If aligned	stMTs	l_0†
v^- ↑	↓	A → D	–‡	∼§	↑
v^+ ↑	↑	D → A	S_2 ↑	↓	↑
r_r ↑	↑	D → A	—	—	—
v^t ↑	↓	A → D	S_2 ↑	↑	↓
r_c ↑	↓	A → D	N/A*	N/A	N/A
r_x ↑	N/A	D → A	S_2 ↓*	↑	N/A

*Through r_c, where applicable. †Theoretical average equilibrium length of noninteracting MTs. ‡Dash denotes no change. §Negligible change.

and 36; see also *SI Appendix*, Fig. S2*A*), and contained fewer long MTs (*SI Appendix*, Fig. S1).

Severing both crossed-over and crossing MTs has a neutral or weakly positive effect on alignment. We then incorporated the experimentally observed preference for severing at crossovers (24, 26, 31) into our simulations using a constant rate r_x (per second) per intersection. Per event, either the crossed or the crossing MT bundle was selected with equal probability, upon which one MT within that bundle was severed ("aselective crossover severing"). With the default parameters, this mode of severing had very little effect on alignment propensity (Fig. 1*C*). To investigate whether this mode of severing is truly without impact, or whether two opposing effects happened to cancel out each other with the default probability $P_{cat} = 0.5$ of having an induced catastrophe, we repeated these simulations with $P_{cat} = 0.09$. Strikingly, aselective crossover severing now resulted in a marked increase in the average degree of alignment close to $G_c = 0$ (*SI Appendix*, Fig. S3*B*). The degree of alignment, however, was much lower than with $P_{cat} = 0.5$, and alignment was unstable (*SI Appendix*, *Unstable Alignment with Aselective Crossover Severing* and Fig. S3 *C–J*). In conclusion, aselective crossover severing has, at best, a weakly positive effect on alignment, or no impact at all.

Preferential severing of crossing MTs at crossovers strongly enhances alignment. All current experimental measurements show a strong bias toward severing the crossing MT rather than the crossed-over one: 97% vs. 3% (24), 330 vs. 192 events (26). Concentrating all severing events to the crossing MTs at crossovers ("crossing-only severing") resulted in a significant increase of the parameter regime of spontaneous alignment compared with no severing (Fig. 1 *D* and *E*). When varying the severing bias at crossovers between the aselective and crossing-only variants, the size of the aligned regime increased gradually with increasing preference for the crossing MT (F_t) (*SI Appendix*, Fig. S4).

Shallow-Angle Interactions Must Be Protected from Severing. The original survival-of-the-aligned mechanism works by selective punishment of discordant MTs. Combining the results with random severing and crossing-only severing in this context suggests the following mechanism for enhancing alignment: (*i*) severing acts as a punishment of MTs (Fig. 1*B*), although weaker than induced catastrophes, because, initially, a leading growing MT bit remains beyond the crossover; (*ii*) when severing primarily affects the crossing MTs at crossovers, this punishment is mostly targeted to discordant MTs; and (*iii*) severing then confers additional punishment of discordant MTs, on top of induced catastrophes, so the parameter regime of spontaneous alignment is increased.

If this mechanism is true, then crossing-only severing will only promote alignment if it is, indeed, primarily affecting discordant MTs. In our simulations thus far, this requirement is met, because collision angles of $<40^\circ$ all result in bundling. Consequently, there are no crossovers with angles of $<40^\circ$, so no "delayed punishment" through severing is possible for these interactions. Previous work without severing shows that alignment is still possible when bundling is replaced by crossovers (16, 18). This change in dynamics, however, exposes shallow-angle interactions to crossover severing, which would be detrimental to ordering; this is, indeed, what we observed (Fig. 2*A*), in stark contrast to Fig. 1*D* with bundling.

In the same vein, crossing-only severing should promote alignment, also without bundling, if shallow-angle crossovers are somehow protected from severing. To test this prediction, we introduced a "protected angle" θ_p, below which no severing occurs; with this, we included crossing-only severing in the theory by ref. 17 as an α-times-weaker form of punishment than induced catastrophes. This approach is supported by the shapes of MT length distributions (*SI Appendix*, *MT Length Distributions* and Fig. S2) and the way in which the severing rate affects the aligned regime (*SI Appendix*, *Increasing Crossing-Only Severing Rates* and Fig. 3).

This theoretical consideration predicted a transition from a detrimental effect on alignment to a positive effect on alignment (at $\theta_p \approx 38^\circ$) with increasing θ_p (Fig. 2*B*). We confirmed this reversal of effects with simulations θ_p (Fig. 2*C*). The maximum enhancement of alignment was even more pronounced with more crossovers ($P_{cat} = 0.09$; *SI Appendix*, Fig. S5).

These results suggest that bundling plays a critical role in supporting katanin action: Bundling concentrates katanin

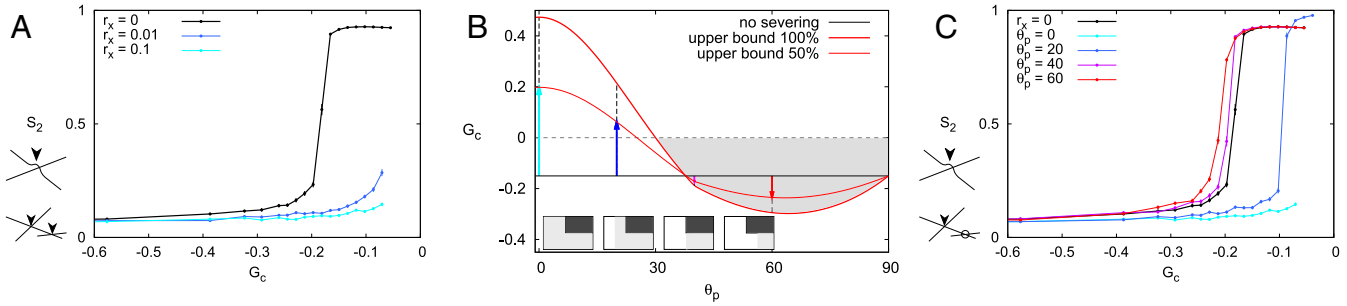

Fig. 2. Bundling normally protects nearly aligned MTs from crossover severing. (*A*) Without bundling, severing at crossovers is detrimental to MT alignment. (*B*) The theoretically estimated effect of protecting angles less than θ_p from severing: Spontaneous alignment may occur in the gray area ($0 > G_c > G^*$). The thick red curve assumes that severing at intersections is equally effective as direct induced catastrophes, an assumption that necessarily overestimates their effectiveness and thus provides an upper bound. The thin red curve shows predictions for 50% effectiveness, illustrating the nonlinear approach toward this theoretical maximum. The cartoons at the bottom show the interaction functions used for *C* corresponding to the colored arrows: dark gray represents induced catastrophes, light gray represents crossovers that may be severed later, and white represents crossovers that are protected from severing. (*C*) The negative effect of crossing-only severing on alignment decreases if shallow angles (below $\theta_p = 20^\circ$, 40°, and 60°) are protected from severing and turns into a positive effect for $\theta_p = 40^\circ$ and 60°. With less frequent induced catastrophes ($P_{cat} = 0.09$), the potential impact of crossing-only severing is even larger (*SI Appendix*, Fig. S5). Error bars represent SEM, with $n = 100$ independent simulations per data point.

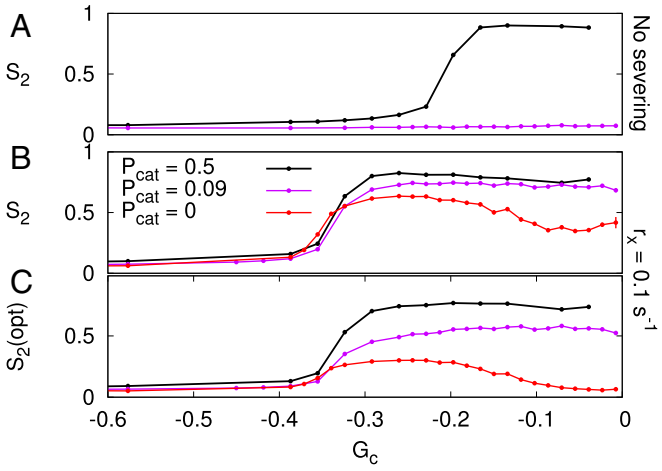

Fig. 3. Crossing-only severing is essential for alignment if induced catastrophes are rare, but is insufficient if they are absent. Bundling occurs for $\theta < 40°$. (*A*) Without severing, the reduced induced catastrophe probability $P_{cat} = 0.09$ is insufficient to find an aligned regime. (*B*) With high severing ($r_x = 0.1\ s^{-1}$), some degree of alignment occurs over the same range of parameters for all three values of P_{cat}. (*C*) Using optical instead of normal S_2 to measure alignment, i.e., counting every stretch of MT bundle as a single MT, regardless of the actual number in the bundle, alignment disappears toward $G_c = 0$ in the absence of induced catastrophes. Also, for intermediate values of G_c, the arrays would appear poorly aligned. Error bars represent SEM, with $n = 100$ independent simulations per data point. For other values of r_x and buildup of alignment over time, see *SI Appendix*, Figs. S6–S8.

severing to large-angle interactions by preventing the occurrence of shallow-angle crossovers.

Crossing-Only MT Severing Requires Subsequent Catastrophes to Promote Alignment. Treating crossing-only severing as a weak form of induced catastrophes raises two questions: (*i*) Does the effectiveness of crossing-only severing depend on induced catastrophes? (*ii*) Can crossing-only severing also induce alignment independently, i.e., without induced catastrophes? Central to these questions is the mechanism that removes the leading MT fragments after severing. What is the relative contribution in this removal of induced catastrophes, spontaneous catastrophes, and a combination of bundling (to adopt the majority orientation) and minus end treadmilling? We investigated the importance of catastrophes by repeating the crossing-only severing simulations (with bundling) of Fig. 1*D* with fewer ($P_{cat} = 0.09$) and no ($P_{cat} = 0$) induced catastrophes. With $P_{cat} = 0.09$, as with the default $P_{cat} = 0.5$, we found a well-aligned regime for the high severing rates ($r_x = 0.01\ s^{-1}$ and $r_x = 0.1\ s^{-1}$), albeit with a somewhat reduced maximum average degree of alignment (Fig. 3 and *SI Appendix*, Fig. S6). Without any induced catastrophes, the maximum degree of alignment further declined. Moreover, the "optical" version of the S_2 alignment parameter—for which each bundle is counted as a single MT, regardless of how many MTs are part of it—was much lower still. Particularly the arrays with $r_x = 0.01\ s^{-1}$ would visually appear disordered over the entire parameter range (*SI Appendix*, Figs. S7 and S8).

We conclude that, in the absence of induced catastrophes, crossing-only severing can, at best, induce a low to moderate degree of alignment. Furthermore, such alignment could only be induced if G_c is not too high, that is, if sufficiently many spontaneous catastrophes occur. This result means that crossing-only severing can only induce alignment with help of enough catastrophes.

Severing and MT Stability. To allow the reader to predict how various mutations and chemical treatments affecting MT stability interact with katanin-mediated severing, we varied each of the remaining parameters: rescue rate (r_r), plus end growth (v^+) and shrinkage (v^-) velocity, and minus end retraction velocity (v^t). In the absence of severing, such changes are accounted for in the survival-of-the-aligned theory ["primary effect" in Table 1; either a switch from disordered (D) to aligned (A) is possible, or the reverse]. That is, they affect G_c (MT length and array density) in such a way that the critical value G^* for the transition between disorder and alignment remains the same. The presence and magnitude of crossing-only severing did not change this finding (*SI Appendix*, Figs. S9 and S10 and Table 1). We noted, however, increased maximum S_2 levels with increasing v^t and, very mildly, also with increasing v^+, but not with r_r or v^-. Increasing v^t thus could have two effects: complete loss of alignment if G_c becomes too small, or increased alignment. Ref. 37 suggested that short treadmilling MTs (stMTs) could enhance alignment, so we quantified the MT length distributions of MTs that grow against the majority orientation (*SI Appendix*, *Measuring Length Distributions of Discordant MT Populations*, Figs. S11 and S12, and Table S2). We found that, even when we fixed the value of G_c (through r_c), the simulations with high v^t had more discordant short MT segments ($< 1.6\mu m$) and fewer long ones. We also observed an increase in short MTs with decreasing v^+, but this was accompanied by a small decrease in maximum S_2. Increasing r_x also increased the abundance of the shortest MTs and decreased maximum S_2 levels (Fig. 4 and *SI Appendix*, Fig. S11 *E* and *F*). Increases in stMT abundance occurred both correlated and anticorrelated with increases in maximum alignment, so this class of MTs is not a significant driver of array alignment in our simulations.

Discussion

Supported by our simulations, we have extended the theory underlying the survival-of-the-aligned mechanism for spontaneous alignment of plant cortical MTs (17, 35), to explain two previously conflicting findings: (*i*) the theoretical finding that katanin-mediated MT severing reduces average MT length, which should result in less alignment (29), and (*ii*) the experimental observations that katanin-mediated severing critically contributes to normal alignment in plants (19, 20, 22, 38).

The core of the survival-of-the-aligned mechanism is that spontaneous alignment occurs if the amount of interactions

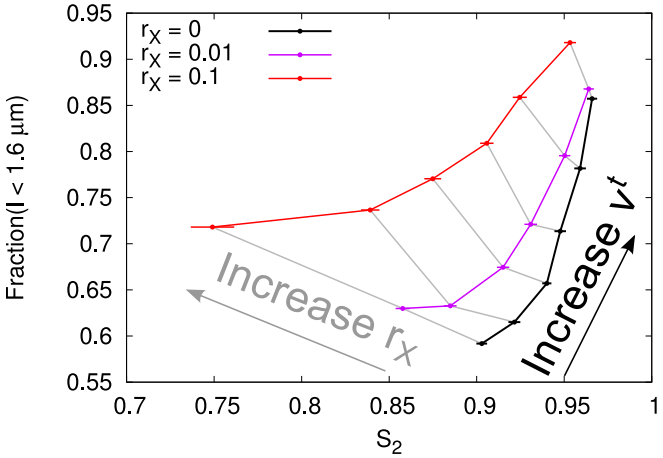

Fig. 4. Opposite correlations between order and short MTs for crossing-only severing and minus end treadmilling. Increasing v^t resulted in increased S_2 and increased the fraction of short MTs (<1.6 μm) with and without crossing-only severing (three curves as indicated in legend). For any given value of v^t, increasing r_x resulted in an increase of the short MTs but a decrease of S_2. The v^t ranges from 0.01 to 0.06 μm/s, and identical values of v^t are connected by gray lines (*SI Appendix*, *Measuring Length Distributions of Discordant MT Populations*).

exceeds a threshold, and this happens only if discordant MTs, i.e., growing against the majority direction, are sufficiently "punished"; this results in a difference in average MT life time between discordant and concordant (i.e., aligned) MTs, which in turn causes the isotropic (i.e., disordered) state to become unstable, thus driving spontaneous alignment.

Our simulations using random severing confirm that severing acts as a punishment, i.e., leads to reduced MT lengths and lifetimes; this only happens because the newly formed plus end starts in the shrinking state, as is observed in vitro (27, 28). We have found that only when severing occurs at crossovers and specifically targets the crossing MTs, the difference between concordant and discordant MTs is enhanced. These conditions are experimentally observed: In *Arabidopsis*, MT severing predominantly occurs at MT crossover sites (24, 26, 31) and predominantly affects the crossing MTs (24, 26). The observed biases were sufficient to enhance alignment in our model.

Our mechanistic approach allowed us to uncover a major hidden requirement of severing enhanced alignment: shallow-angle encounters must be protected from severing. This protection naturally occurs through bundling, as is supported by our simulations without bundling (Fig. 2). Experiments from two independent labs support that the katanin-mediated severing rate is independent of the crossover angle (24, 26), suggesting that bundling is required for this protection. Together, this provides a mechanistic explanation of why MT bundling may be essential for the self-organization of the plant cortical MT array in real cells.

Our simulations show that MT severing, depending on the model parameters, can induce MT ordering (Fig. 1*D*). This finding suggests that MT severing is a potential target for regulating MT organization in vivo. Interestingly, overexpressing the p60 subunit of the katanin complex can lead to progressive loss of MT length and alignment in *Arabidopsis* (39), suggesting a proper balance between catalytic (p60) and regulatory (p80) katanin subunits is crucial for normal MT organization. Other experimental data suggest that katanin-mediated severing activity can be regulated through interactions between RIC1 and katanin p60 (30), and in a blue light-dependent manner through photoreceptors PHOT1/PHOT1 (26). Moreover, the MT array responds far less to mechanical perturbations in *katanin* loss-of-function mutants (25). All of these findings suggest that tuning MT severing is indeed an important target for responding to environmental stimuli and changing MT organization (40).

The stMTs were absent in the *katanin* loss-of-function mutant (37); this can be understood from the fact that katanin not only severs MTs at crossovers, but is also responsible for their release from nucleation sites (32). Without either process, few treadmilling MTs are expected. Ref. 37 reported a twofold to threefold increase in the abundance of stMTs in the *spr2* mutant petiole cells. SPR2 is proposed to protect crossover sites from severing (23). Our simulations, however, cannot explain the increased stMT abundance in *spr2* by increasing r_x alone, because this produced only a small increase in stMT abundance and was correlated with a decrease of alignment. It is, however, conceivable that stMTs could play a role in MT organization because of factors such as MT age and/or length-dependent properties that affect MT reorientation and are not accounted for in our simulations. Once such effects have been firmly experimentally established, it will be interesting to incorporate them. We found that substantial changes in v^t or v^+ produced a change in stMT abundance of the experimentally observed magnitude, and, only with v^t, this change correlated with increased alignment (*SI Appendix*, Figs. S11 and S12). Our results thus suggest that MT treadmilling properties are potentially potent targets for controlling MT organization.

During blue light reorientation of the hypocotyl array, a subpopulation of severing-created plus ends started in the growing state, and 1.7 times as many severing events affected the crossing MTs of the new (longitudinal) orientation (26). In terms of our framework, this renders katanin-mediated severing as an amplifier rather than repressor of the discordant (longitudinal) MT population, exactly what is needed to initiate reorientation. Additional enhancement of the discordant MT population could occur if the cell would temporarily enter the unbound growth regime, as this hampers the removal of leading MT stubs (Fig. 3). This regime could be reached by decreasing the spontaneous catastrophe rate and/or shrinkage velocity and/or increasing the growth velocity and/or rescue rate. Neither option, however, imposes a final directionality to the array, so a complete reorientation requires additional mechanism(s) to favor and fix the new orientation. Which of different possible mechanisms are involved in a particular type of reorientation remains a topic for further investigation.

In conclusion, our work provides mechanistic understanding of the role of MT severing in MT alignment, and why MT severing is an excellent target to induce changes in MT organization in vivo. Our results, moreover, encourage measurements of minus end treadmilling parameters in mutants that show MT organization phenotypes.

Materials and Methods

Basic Simulation Methods and Parameters. All simulations have been carried out using CorticalSim version 1.26.1 (16); this is a fast, event-based simulation platform that explicitly includes all individual MTs. MTs can grow straight at their plus ends with $v^+ = 0.08\ \mu m{\cdot}s^{-1}$, or shrink with $v^- = 0.16\ \mu m{\cdot}s^{-1}$. They can switch between these states with catastrophe rate r_c and rescue rate $r_r = 0.007\ s^{-1}$, respectively (41). All minus ends show steady retraction (treadmilling) with $v^t = 0.01\ \mu m{\cdot}s^{-1}$ (12). New MTs are nucleated with a uniform isotropic nucleation rate of $r_n = 0.001\ \mu m^{-2}$. The effect of MT–MT collisions depends on the relative angle θ. For $\theta < \theta^* = 40°$, bundling occurs. For larger angles, induced catastrophes occur with probability P_{cat}, or the MTs cross over one another (Fig. 1*A*). The same interaction function is also used by other researchers, with varying values for P_{cat} (14, 15). These basic dynamic parameters are the same as in our previous simulation studies (16, 33, 34). We have used a periodic $80 \times 80\ \mu m^2$ simulation domain, i.e., with dimensions similar to a plant cell circumference. Source code is available (42).

Modes of Katanin Action. In all cases, a severing event results in the severing of a single MT. The newly formed MT plus end starts in the shrinking state, and the newly formed minus end immediately starts treadmilling. In the "random" mode, katanin severs MTs with a constant rate per unit length r_s (per micrometer per second); this makes the computation of simulation events dependent on the, continuously varying, total MT length density. For technical details, see the supporting information of ref. 16.

In the crossover mode, intersections are severed with constant rate r_x (s^{-1}) per intersection. Zhang et al. (24) reported an average waiting time until severing of 41 s ± 14 s in transverse arrays (mode: <40 s), indicating that our highest used rate of $r_x = 0.1\ s^{-1}$ is high but still in a realistic ballpark. Typically, a single MT is selected for severing from the bundle (possibly consisting of one MT only) that arrived second at the intersection. We call this "crossing-only severing." The second bundle usually corresponds to the bundle on the cytoplasmic side of the intersection. We also performed "aselective crossover severing" simulations in which either bundle was selected at random (Fig. 1*C* and *SI Appendix*, Fig. S3), upon which a single MT from the selected bundle was severed.

We introduced a protected angle θ_p below which no severing occurs. This modification is only used in Fig. 2 and *SI Appendix*, Fig. S5, whereas, in the default simulations, the presence of bundling effectively results in a protected angle of 40°.

Measuring Alignment: S_2. To measure the degree of alignment, we use the planar S_2 order parameter (16, 33),

$$S_2 = \frac{\sqrt{\left[\sum_n l_n \cos(2\theta_n)\right]^2 + \left[\sum_n l_n \sin(2\theta_n)\right]^2}}{\sum_n l_n}, \quad [1]$$

with l_n as the length of individual MT segments and θ_n as the absolute orientation of the segment within the simulation domain. S_2 increases monotonically from 0 (perfectly isotropic system) to 1 (all MTs with exactly the same orientation, disregarding segment polarity). A corresponding angle θ_{S_2} indicates the orientation of the alignment and takes values from $-\pi/2$ to $\pi/2$ (−90 to 90°).

Control Parameter G_c. Control parameter G_c, which combines all dynamic instability parameters and the nucleation rate, was originally derived without minus end treadmilling (17, 18) and has subsequently been extended to include treadmilling in the absence of MT bundling (33),

$$G_c = \sqrt[3]{\frac{2(v^+ - v^t)^2(v^- + v^t)}{r_n v^+(v^+ + v^-)}}\left(\frac{r_r}{v^- + v^t} - \frac{r_c}{v^+ - v^t}\right). \quad [2]$$

For $G_c \geq 0$, there is no intrinsic bound on MT growth, which, in practice, results in an absence of steady-state solutions with biologically relevant densities, so that natural systems can, at most, transiently exist with $G_c \geq 0$. We use parameter $r_c \in [0.003\ s^{-1}, 0.02\ s^{-1}]$ to vary G_c, which we emphasize using the subscript c. With our default parameters, $G_c \approx -63.2s\, r_c + 0.182$.

Critical Value G^* of G_c. The mean field theory in Hawkins et al. (18) predicts that the system will align for $G_c > G^*$, and not for smaller G_c. The biologically relevant range for alignment is thus $G^* < G_c < 0$. In the absence of severing, the value of G^* depends on the zeroth and second Fourier coefficient of interaction function as

$$G^* = \sqrt[3]{-2\hat{c}_2}\left(\frac{\hat{c}_0}{-2\hat{c}_2} - 1\right), \quad [3]$$

with

$$\hat{c}_n = \frac{4}{\pi}\int_0^{\pi/2} \sin(\theta)\cos(n\theta)P_{cat}(\theta)\mathrm{d}\theta \quad [4]$$

and θ as the (relative) collision angle (16).

Due to the spatial correlations that typically occur in real (and simulated) cells, the transition between isotropic and aligned states typically deviates somewhat from the theoretical value, but G^* remains a powerful concept to predict the direction of change (16).

To predict the effects of crossing-only severing in the absence of bundling, we assume that it effectively functions as an $0 < \alpha \leq 1$ times-as-effective induced catastrophe, based on the detrimental effects random severing on alignment. This results in

$$\hat{c}_n = \frac{4}{\pi}\int_0^{\pi/2} \sin(\theta)\cos(n\theta)\left\{P_{cat}(\theta) + \alpha\left[1 - P_{cat}(\theta)\right]q(\theta > \theta_p)\right\}\mathrm{d}\theta, \quad [5]$$

with $q(\theta > \theta_p)$ as a step function that is 1 for collision angles larger than protected angle θ_p and zero otherwise.

ACKNOWLEDGMENTS. We thank Pier Siersma for his input during the initial stages of this work. The work of B.M.M. is part of the research program of the Foundation for Fundamental Research on Matter, which is part of the Netherlands Organisation for Scientific Research.

1. Xu T, et al. (2010) Cell surface- and rho gtpase-based auxin signaling controls cellular interdigitation in *Arabidopsis*. *Cell* 143:99–110.
2. Vermeer JEM, et al. (2014) A spatial accommodation by neighboring cells is required for organ initiation in *Arabidopsis*. *Science* 343:178–183.
3. Gutierrez R, Lindeboom JJ, Paredez AR, Emons AM, Ehrhardt DW (2009) *Arabidopsis* cortical microtubules position cellulose synthase delivery to the plasma membrane and interact with cellulose synthase trafficking compartments. *Nat Cell Biol* 11:797–806.
4. Paredez A, Somerville C, Ehrhardt D (2006) Visualization of cellulose synthase demonstrates functional association with microtubules. *Science* 312:1491–1495.
5. Ehrhardt D (2008) Straighten up and fly right – Microtubule dynamics and organization of non-centrosomal arrays in higher plants. *Curr Opin Cell Biol* 20:107–116.
6. Hamant O, et al. (2008) Developmental patterning by mechanical signals in *Arabidopsis*. *Science* 322:1650–1655.
7. Shibaoka H (1994) Plant hormone-induced changes in the orientation of cortical microtubules: Alterations in the cross-linking between microtubules and the plasma membrane. *Annu Rev Plant Biol* 45:527–544.
8. Bouck GB, Ngo H (1996) Cortical structure and function in euglenoids with reference to trypanosomes, ciliates, and dinoflagellates. *Int Rev Cytol* 169:267–318.
9. Reilein A, Yamada S, Nelson WJ (2005) Self-organization of an acentrosomal microtubule network at the basal cortex of polarized epithelial cells. *J Cell Biol* 171:845–855.
10. Elinson RP, Rowning B (1988) A transient array of parallel microtubules in frog eggs: Potential tracks for a cytoplasmic rotation that specifies the dorso-ventral axis. *Dev Biol* 128:185–197.
11. Desai A, Mitchison TJ (1997) Microtubule polymerization dynamics. *Annu Rev Cell Dev Biol* 13:83–117.
12. Shaw S, Kamyar R, Ehrhardt D (2003) Sustained microtubule treadmilling in *Arabidopsis* cortical arrays. *Science* 300:1715–1718.
13. Dixit R, Cyr R (2004) Encounters between dynamic cortical microtubules promote ordering of the cortical array through angle-dependent modifications of microtubule behavior. *Plant Cell* 16:3274–3284.
14. Allard JF, Wasteneys GO, Cytrynbaum EN (2010) Mechanisms of self-organization of cortical microtubules in plants revealed by computational simulations. *Mol Biol Cell* 21:278–286.
15. Eren EC, Dixit R, Gautam N (2010) A 3D computer simulation model reveals the mechanisms for self-organization of plant cortical microtubules into oblique arrays. *Mol Biol Cell* 21:2674–2684.
16. Tindemans SH, Deinum EE, Lindeboom JJ, Mulder B (2014) Efficient event-driven simulations shed new light on microtubule organisation in the plant cortical array. *Front Phys* 2:9.
17. Tindemans SH, Hawkins RJ, Mulder BM (2010) Survival of the aligned: Ordering of the plant cortical microtubule array. *Phys Rev Lett* 104:058103.
18. Hawkins RJ, Tindemans SH, Mulder BM (2010) Model for the orientational ordering of the plant microtubule cortical array. *Phys Rev E* 82:011911.
19. Burk D, Liu B, Zhong R, Morrison W, Ye Z (2001) A katanin-like protein regulates normal cell wall biosynthesis and cell elongation. *Plant Cell* 13:807–828.
20. Bichet A, Desnos T, Turner S, Grandjean O, Höfte H (2001) Botero1 is required for normal orientation of cortical microtubules and anisotropic cell expansion in *Arabidopsis*. *Plant J* 25:137–148.
21. Stoppin-Mellet V, Gaillard J, Vantard M (2002) Functional evidence for in vitro microtubule severing by the plant katanin homologue. *Biochem J* 365:337–342.
22. Bouquin T, Mattsson O, Naested H, Foster R, Mundy J (2003) The *Arabidopsis lue1* mutant defines a katanin p60 ortholog involved in hormonal control of microtubule orientation during cell growth. *J Cell Sci* 116:791–801.
23. Wightman R, Chomicki G, Kumar M, Carr P, Turner SR (2013) Spiral2 determines plant microtubule organization by modulating microtubule severing. *Curr Biol* 23:1902–1907.
24. Zhang Q, Fishel E, Bertroche T, Dixit R (2013) Microtubule severing at crossover sites by katanin generates ordered cortical microtubule arrays in *Arabidopsis*. *Curr Biol* 23:2191–2195.
25. Uyttewaal M, et al. (2012) Mechanical stress acts via katanin to amplify differences in growth rate between adjacent cells in *Arabidopsis*. *Cell* 149:439451.
26. Lindeboom JJ, et al. (2013) A mechanism for reorientation of cortical microtubule arrays driven by microtubule severing. *Science* 342:1245533–1245533.
27. Walker RA, Inoué S, Salmon ED (1989) Asymmetric behavior of severed microtubule ends after ultraviolet-microbeam irradiation of individual microtubules in vitro. *J Cell Biol* 108:931–937.
28. Tran PT, Walker RA, Salmon ED (1997) A metastable intermediate state of microtubule dynamic instability that differs significantly between plus and minus ends. *J Cell Biol* 138:105–117.
29. Tindemans SH, Mulder BM (2010) Microtubule length distributions in the presence of protein-induced severing. *Phys Rev E* 81:031910.
30. Lin D, et al. (2013) Rho GTPase signaling activates microtubule severing to promote microtubule ordering in *Arabidopsis*. *Curr Biol* 23:290–297.
31. Wightman R, Turner S (2007) Severing at sites of microtubule crossover contributes to microtubule alignment in cortical arrays. *Plant J* 52:742–751.
32. Nakamura M, Ehrhardt DW, Hashimoto T (2010) Microtubule and katanin-dependent dynamics of microtubule nucleation complexes in the acentrosomal *Arabidopsis* cortical array. *Nat Cell Biol* 12:1064–1070.
33. Deinum EE, Tindemans SH, Mulder BM (2011) Taking directions: The role of microtubule-bound nucleation in the self-organization of the plant cortical array. *Phys Biol* 8:056002.
34. Lindeboom JJ, et al. (2013) Cortical microtubule arrays are initiated from a nonrandom prepattern driven by atypical microtubule initiation. *Plant Physiol* 161:1189–1201.
35. Deinum EE, Mulder BM (2013) Modelling the role of microtubules in plant cell morphology. *Curr Opin Plant Biol* 16:688–692.
36. Dogterom M, Leibler S (1993) Physical aspects of the growth and regulation of microtubule structures. *Phys Rev Lett* 70:1347–1350.
37. Chomicki G, Wightman R, Turner SR (2016) A specific class of short treadmilling microtubules enhances cortical microtubule alignment. *Mol Plant* 9:1214–1216.
38. Webb M, Jouannic S, Foreman J, Linstead P, Dolan L (2002) Cell specification in the *Arabidopsis* root epidermis requires the activity of ectopic root hair 3-a katanin-p60 protein. *Development* 129:123131.
39. Stoppin-Mellet V, Gaillard J, Vantard M (2006) Katanin's severing activity favors bundling of cortical microtubules in plants. *Plant J* 46:1009–1017.
40. Nakamura M (2015) Microtubule nucleating and severing enzymes for modifying microtubule array organization and cell morphogenesis in response to environmental cues. *New Phytol* 205:1022–1027.
41. Vos J, Dogterom M, Emons A (2004) Microtubules become more dynamic but not shorter during preprophase band formation: A possible "search-and-capture" mechanism for microtubule translocation. *Cell Motil Cytoskeleton* 57:246–258.
42. Tindemans SH, Deinum EE (2017) Data from "Corticalsim v1.26.1." *Zenodo*. https://dx.doi.org/10.5281/zenodo.801851.

SI appendix for: How selective severing by katanin promotes order in the plant cortical microtubule array

Eva E. Deinum [*] [†] [‡], **Simon H. Tindemans** [†] [§], **Jelmer J. Lindeboom** [¶] **and Bela M. Mulder** [†] [‖]

[*]Mathematical and Statistical Methods, Wageningen University & Research, 6708 PB Wageningen, The Netherlands, [†]Systems Biophysics, AMOLF, 1098XG Amsterdam, the Netherlands, [¶]Department of Plant Biology, Carnegie Institution for Science, Stanford CA 94305, USA, [‖]Laboratory of Cell Biology, Wageningen University & Research, 6708 PB Wageningen, the Netherlands, [§]Present address: Department of Electrical and Electronic Engineering, Imperial College London, London SW7 2AZ, United Kingdom, and [‡]To whom correspondence should be addressed. Email: eva.deinum@wur.nl

Edited by Olivier Hamant, École Normale Supérieure de Lyon, Lyon, France, and accepted by Editorial Board Member Caroline Dean May 9, 2017 (received for review February 24, 2017)

Supplementary text

T1 Unbiased selection of snapshots (fig. 1E)

To avoid a result driven bias in the selection of snapshots for the overview diagram of fig. 1E, we applied the following automated selection criterion. For each parameter combination, we obtained snapshots (after 30h of simulated time) for 5 independent simulations. Of these, we blindly selected one with median S_2 value of the five.

T2 Unstable alignment with aselective crossover severing and $P_{cat} = 0.09$

In our simulations with crossing-only severing and a low induced catastrophe probability ($P_{cat} = 0.09$), we observed that crossing-only severing could produce at best an intermediate degree of alignment (up to $S_2 \approx 0.4$).

To understand this intermediate degree of alignment we performed a number of extra long simulations of 100 hours (> 4 days). Fig. S3C,D,E shows time traces of the degree of alignment of several individual runs, colored by the overall orientation of the array, and some snapshots of the system of two runs, as indicated by arrows in fig. S3D. Strikingly, these runs do not show the usual pattern of a stable increase of S_2 until some plateau is reached [e.g. see fig. S6C,D and 1; 2], but several periods with intermediate S_2 separated by periods with very low S_2. We also observed that the net orientation of the array in consecutive aligned periods was often different. We noted that the arrays without severing looked similar to those in complete absence of induced catastrophes in that they could locally harbour up to four orientations differing by more than 40° [c.f. fig. S1 in 2], suggesting that with this low value of $P_{cat} = 0.09$, the effect of bundling is so distorting with respect to alignment that the induced catastrophes cannot overcome it (or perhaps only *very* close to $G_c = 0$ and with *very* long equilibration times).

With this implementation of crossover severing, either the crossed over or the crossing bundle is selected for a severing event with equal probability, regardless of the number of MTs in each bundle. In the – not necessarily realistic – regime that severing typically occurs so fast that the number of MTs at the crossover in both bundles remains otherwise unchanged, the expected number of crossed over MTs in a bundle of n that is severed before a single crossing one is $1 - (\frac{1}{2})^n$, which rapidly converges to 1. This calculation allows for the possibility that with low spontaneous catastrophe rates r_c, high crossover severing rates r_x and few/no induced catastrophes, there is a regime in which a single discordant MT is likely to cause multiple severing events of concordant MTs before undergoing an induced catastrophe itself. We hypothesize that this is the basis of the recurring decline of alignment in these systems. Biologically, this would suggest that increasing the fraction of severing events targeting crossed over MTs could aid in the breakdown of an established array orientation.

T3 MT length distributions

Exponential distributions in absence of severing. Early theoretical work on non-interacting MTs in absence of severing predicts an exponential length distribution [3]. This prediction is conserved for interacting MTs, even with bundling (but no severing) [4], which we readily confirmed in our simulations (fig. S2A).

More compact distributions with random severing. Theoretical work on non-interacting MTs predicts that random severing leads to more "compact" length distributions, i.e., with fewer long MTs than with an exponential distribution [5]. This happens because random severing occurs with a constant rate (r_s) per unit of MT length, so longer MTs are more likely to get severed somewhere. We also found these compact distributions in our interacting system (fig. S1). The effect was more pronounced with increasing severing rate r_s.

Crossing-only severing results in mostly exponential distributions. With bundling, when crossing-only severing is effective in promoting alignment, we found exponential length distributions (fig. S2B). We did not detect the compacting effect on the length distributions that we saw with random severing. This indicates that this form of severing is not randomly affecting all MTs, but preferentially affects discordant MTs with the same proportionality as induced catastrophes do. This observation thus supports our claim that crossing-only severing promotes alignment in a way similar to induced catastrophes (albeit less effective).

Reserved for Publication Footnotes

Local domain formation affects MT length distributions. It is possible that the system aligns, but forms multiple domains with distinct orientations [fig. 1E; see also 6; 2]. This, of course, interferes with the MT length distributions, for example see (fig. S2C). The distinct peaks in the histogram of the dominant orientation angles correlate with the length of individual domains appeared as peaks in the histogram.

"Mixed" length distributions in absence of bundling. Fig. S2D shows an example of length distributions with crossing-only severing and no bundling. The distributions appear as mixture of the compact distributions created by random severing, particularly for the discordant angles, and exponential, in the tails of the concordant angles, typical of no severing and crossing-only severing in the presence of bundling. In other words: at the concordant angles, all but the shortest length class show an exponential distribution, which indicates they are hardly affected by severing, whereas the other MTs follow a more compact distribution, suggesting severing is frequent among those. This effect occurs because new stretches of MT length are typically crossing at crossovers, and with increasing age, the likelihood of a stretch being the crossed over one increases and, hence, the exposure to severing decreases. Only concordant MTs are likely to get so old that severing ceases over most of their lattice, so the exponential tail is only expected for the majority orientation.

With bundling, on the other hand, concordant MTs are likely to entrain with older MTs soon after their nucleation, which increases their chances of being on an "old" bundle. This difference also explains that we found a larger aligned regime for crossing-only severing with bundling, than without bundling in combination with a protected angle of 40° or 60°.

T4 Increasing crossing-only severing rates make the width of the aligned regime (G^*) less dependent on the induced catastrophe probability (P_{cat})

The survival-of-the-aligned theory predicts that in absence of severing (and regardless of bundling) the width of the aligned regime increases with increasing induced catastrophe probability P_{cat} (i.e., G^* gets smaller). Adding crossing-only severing to the theory as a tunable weaker form of induced catastrophes () yields the prediction that with increasing crossover severing rates r_x, the width of the aligned regime becomes less dependent on P_{cat}. Considering all our simulations with bundling and crossing-only severing together supports that: the location of the onset of the aligned regime is almost the same at high values of r_x, but very different without severing (fig. 3), (all simulations with bundling; separately shown in figures 1D ($P_{cat} = 0.5$), S6A ($P_{cat} = 0.09$), and S7AB and S8AB ($P_{cat} = 0$)).

T5 Measuring length distributions of discordant MT populations

Length distributions were measured based on 100 independent simulations per parameter set. We used a 2D histogram of MT segment orientation (10 bins of 18°width) and length (20 bins). The bins for MT segment length were of equal size per orientation, but their width was adapted dynamically to the length of simulated MT segments: bin widths were scaled successively by a factor of two to accommodate the largest segment. During simulations, histograms were computed as averages of 5 measurements 3 minutes apart.

Observing maximum length of all histograms, we concluded that histograms with a maximum length of 8 μm or less always represented minority orientations, except when changing v^+, where a maximum length of 16 μm was needed. We averaged the MT segment counts of all these "short" histograms per parameter combination (so individual simulations could contribute more than one histogram). Where possible, we used both 8 μm and 16 μm as a maximum. The differences between both were small, and all trends and differences within and between groups were conserved (table S2).

To ensure the same value of $G_c = -0.121729$ for all values of v^t, we adjusted r_c as given below. All other parameters were default values.

v^t $(\mu m/s)$	r_c (s^{-1})	l_0 $(\mu m)^a$
0.01	0.00480707426531	36.4
0.02	0.00412714867275	33.4
0.03	0.0035	30.2
0.04	0.00291296245279	26.4
0.05	0.00235244248501	22.2
0.06	0.00179965165925	17.2

For varying r_r, the following r_c values were used for ensuring the same value of $G_c = -0.121282$

r_r (s^{-1})	r_c (s^{-1})	l_0 (μm)
0.003	0.00315294117647	36.5
0.005	0.00397647058824	36.5
0.007	0.0048	36.5
0.009	0.00562352941176	36.5
0.012	0.00685882352941	36.5

For varying v^+, the following r_c values were used for ensuring the same value of $G_c = -0.121282$. Moreover, the cutoff for the discordant MT orientations was a maximum length of 16 μm, because with the higher values of v^+, little/no shorter histograms occurred.

v^+ $(\mu m/s)$	r_c (s^{-1})	l_0 (μm)
0.05	0.00294838256325	30.7
0.08	0.0048	36.5
0.12	0.00721607300528	40.9
0.16	0.00960485355814	43.7

For varying v^-, the following r_c values were used for ensuring the same value of $G_c = -0.121282$.

v^- $(\mu m/s)$	r_c (s^{-1})	l_0 (μm)
0.08	0.00751525512526	33.8
0.12	0.00574260803081	35.5
0.16	0.0048	36.5
0.20	0.00421478969932	37.2
0.25	0.00373542367372	37.8

Fractions of short MTs are provided in table S2.

[a] l_0 is the theoretical average equilibrium length of non-interacting MTs:

$$l_0 = -1 \Big/ \left(\frac{r_r}{v^- + v^t} - \frac{r_c}{v^+ - v^t} \right) \qquad [1]$$

Supplementary figures

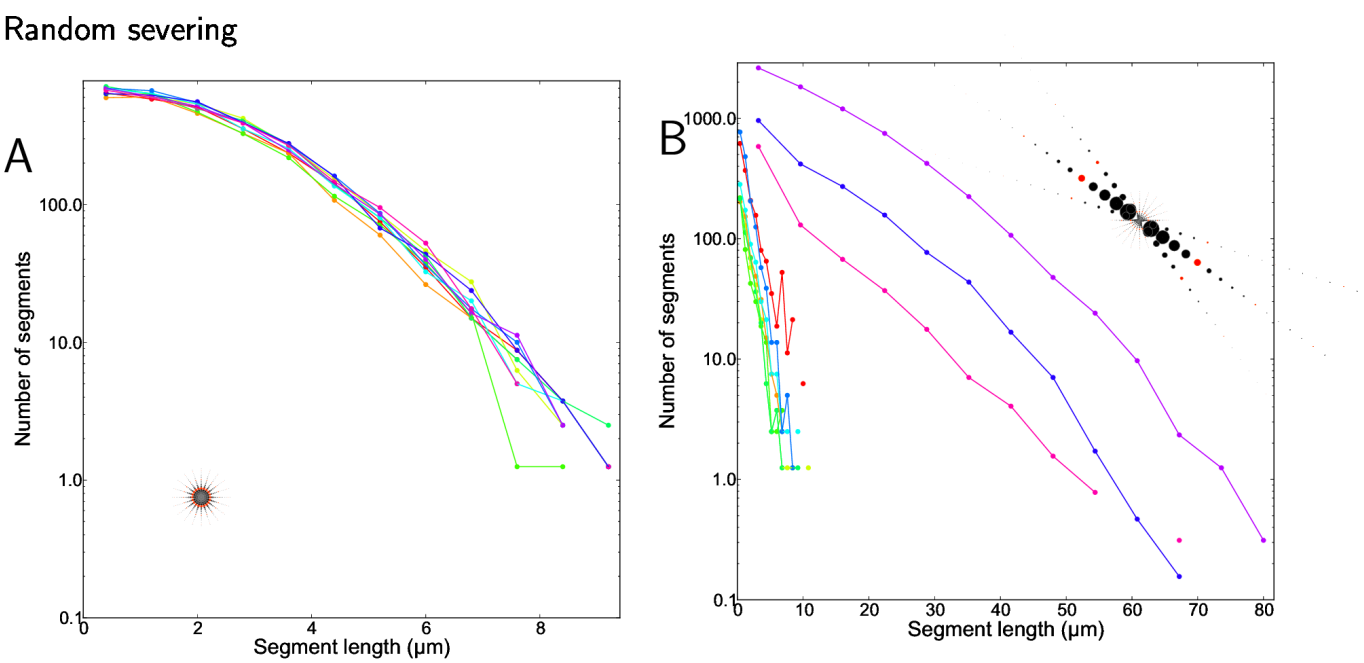

Fig. S1. Example length distributions with random severing. Density of segments with a particular length for 10 equal 18° orientation bins, color coded as in 1E. The y-axis is on a logarithmic scale, so exponential length distributions show as straight lines. A: $r_s = 0.01\ \mu m^{-1}s^{-1}$, $r_x = 0\ s^{-1}$, $r_c = 0.006\ s^{-1}$. B: $r_s = 0.0001\ \mu m^{-1}s^{-1}$, $r_x = 0\ s^{-1}$, $r_c = 0.004\ s^{-1}$. All graphs are averages of ten 3-minute spaced measurements preceding and including 30h. Dotted insets show the orientation of the length histograms with dot surface proportional to the number of segments. All insets are drawn on the same scale.

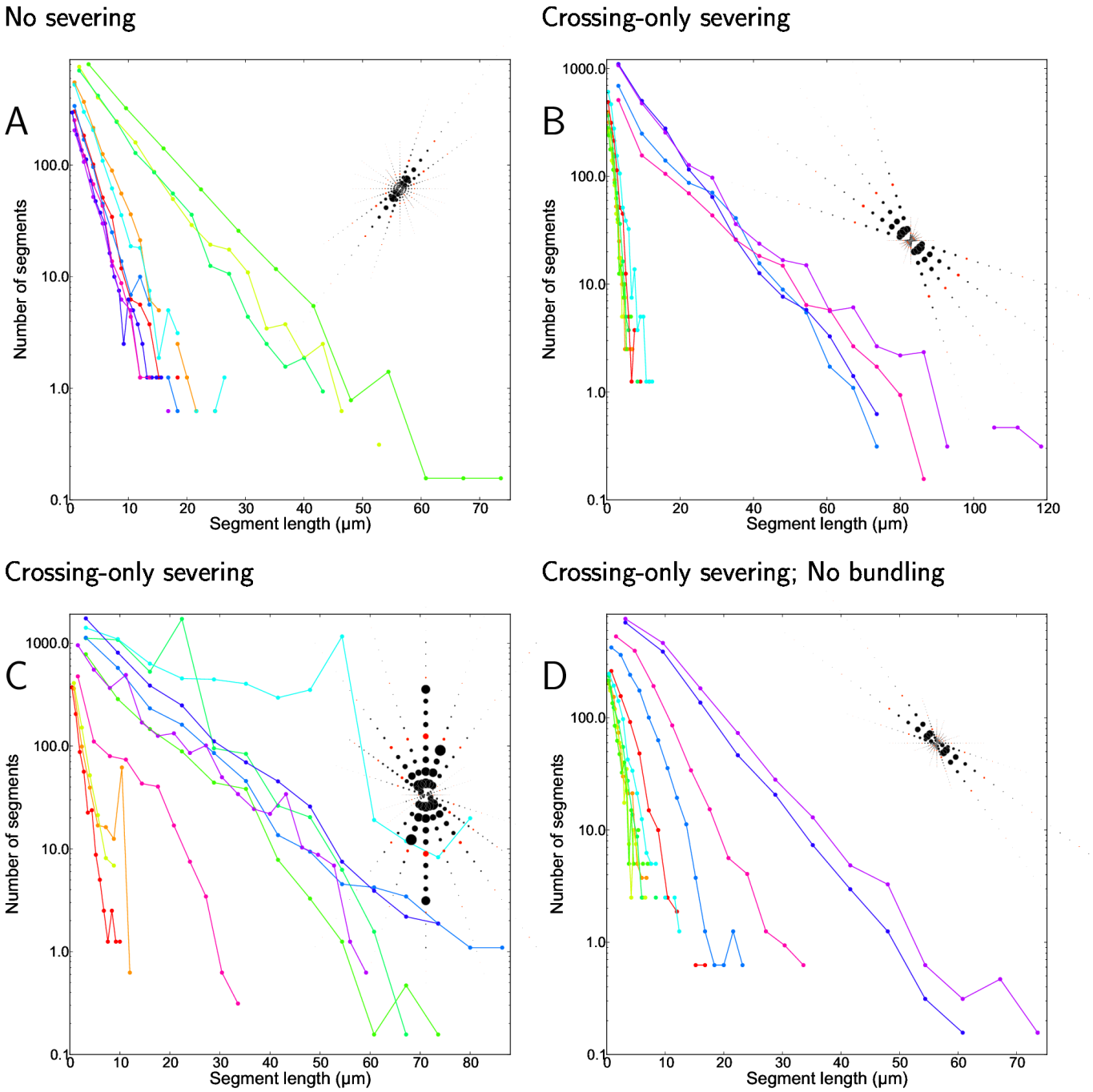

Fig. S2. Example length distributions with no or crossing-only severing. Density of segments with a particular length for 10 equal 18° orientation bins, color coded as in 1E. The y-axis is on a logarithmic scale, so exponential length distributions show as straight lines. A: no severing: $r_s = 0\ \mu m^{-1}s^{-1}$, $r_x = 0\ s^{-1}$, $r_c = 0.006\ s^{-1}$. B: $r_s = 0\ \mu m^{-1}s^{-1}$, $r_x = 0.1\ s^{-1}$, $r_c = 0.006\ s^{-1}$. C: $r_s = 0\ \mu m^{-1}s^{-1}$, $r_x = 0.1\ s^{-1}$, $r_c = 0.004\ s^{-1}$. D: No zippering; $r_s = 0\ \mu m^{-1}s^{-1}$, $r_x = 0.01\ s^{-1}$, $r_c = 0.0035\ s^{-1}$. All graphs are averages of ten 3-minute spaced measurements preceding and including 30h. Dotted insets show the orientation of the length histograms with dot surface proportional to the number of segments. All insets are drawn on the same scale as in fig. S1.

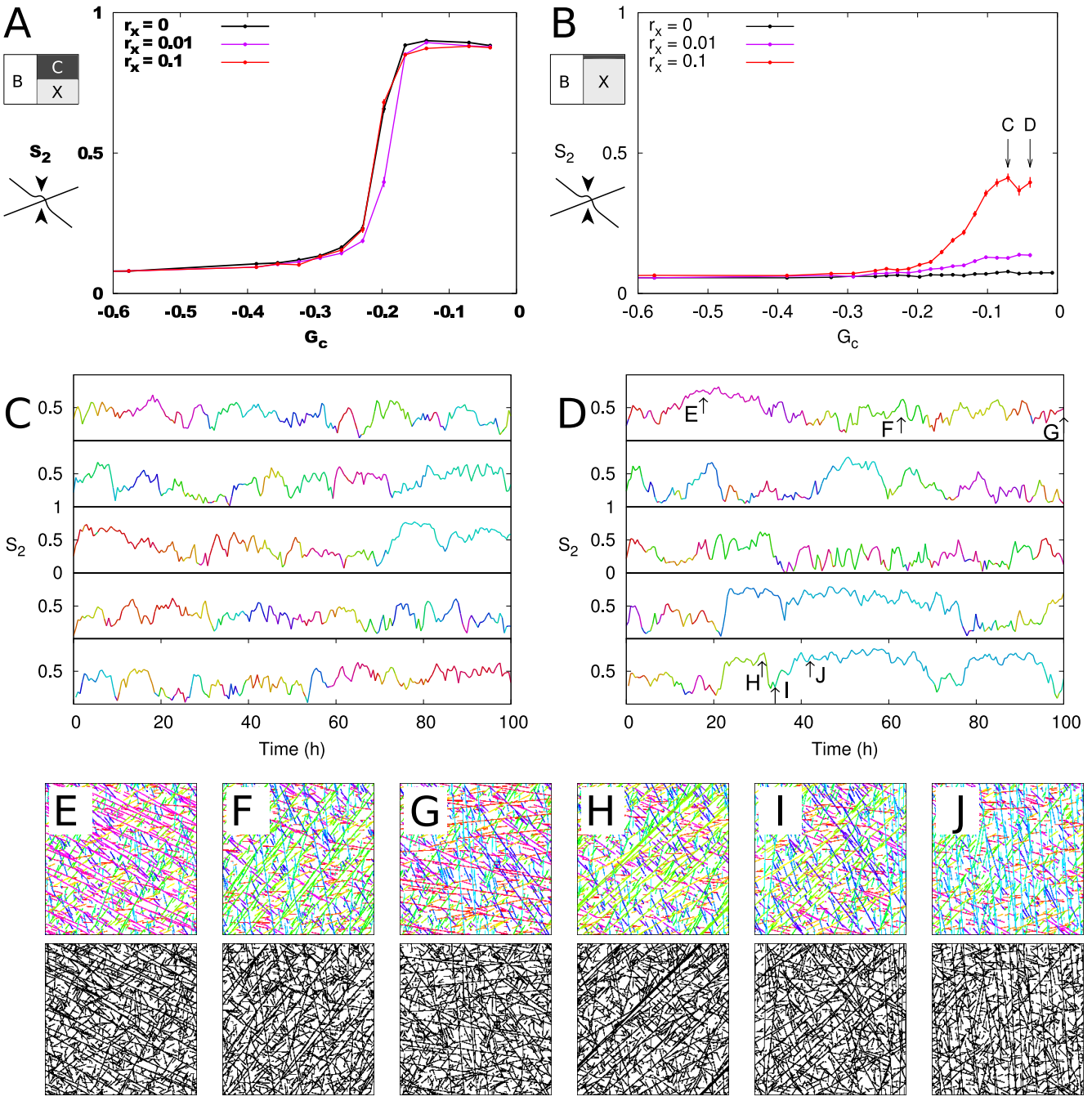

Fig. S3. Aselective severing destabilizes alignment. A,B: severing at crossovers, but randomly selecting the crossed over or crossing MT (bundle) for severing (with bundling). A: $P_{cat} = 0.5$. B: $P_{cat} = 0.09$. Error bars show the SEM with n=100 independent simulations per data point. T=30h. C,D: time traces of S_2 of individual runs from the half-aligned regime of B (up to 100h), colored by array orientation θ_{S_2} on a circular scale as in fig. 1E. $r_x = 0.1\ s^{-1}$, $r_c = 0.004\ s^{-1}$ (C) or $r_c = 0.0035\ s^{-1}$ (D), as indicated with arrows in B. E-J: snapshots of the points indicated with arrows and letters in D.

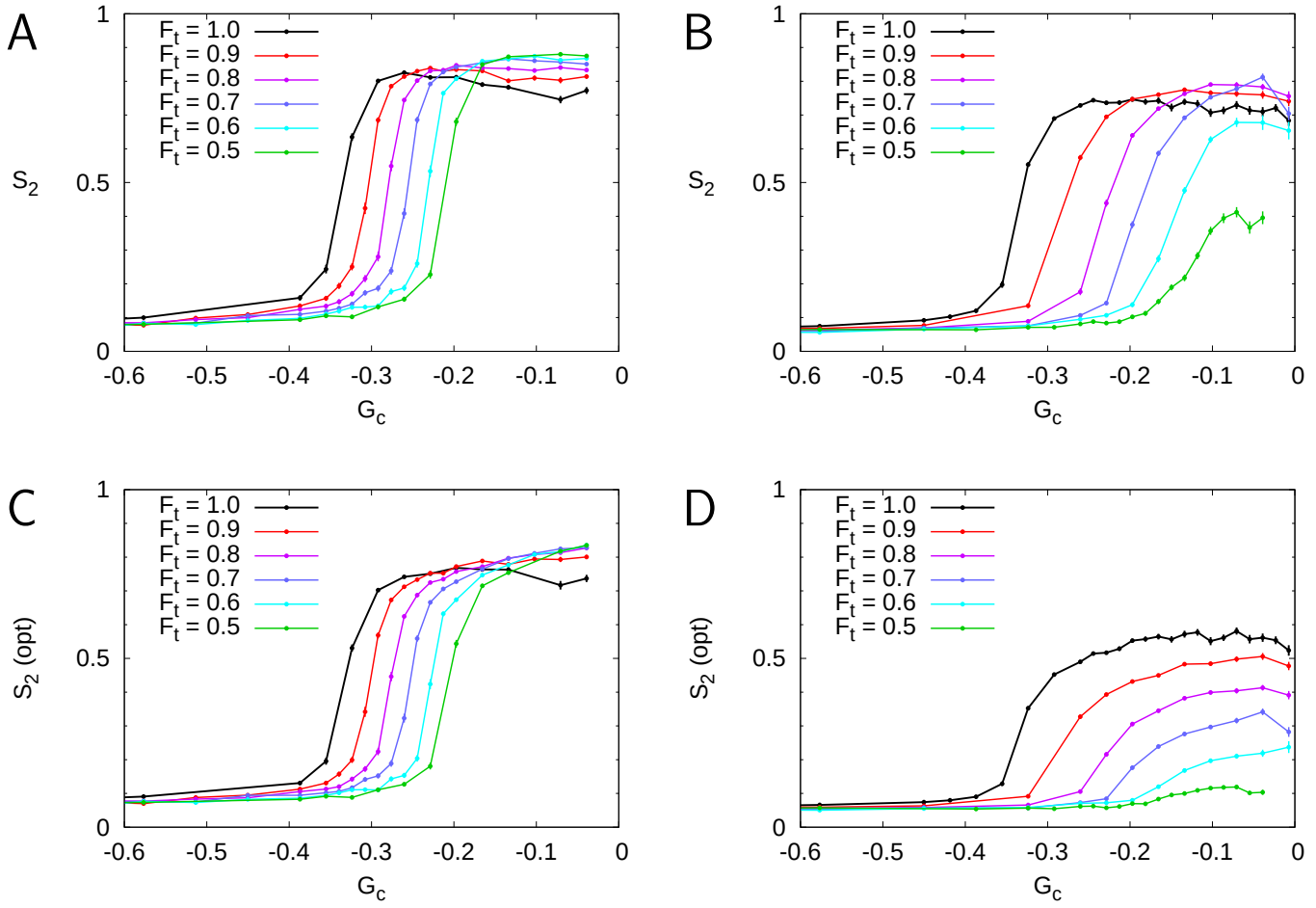

Fig. S4. Transtion between aselective crossover-severing ($F_t = 0.5$) and crossing-only severing ($F_t = 1$) is gradual. At each severing event, severing the crossing MT (bundle) had probability F_t. Figures show G_c, S_2 curves for different values of F_t, as indicated. A,B: regular S_2, C,D: "optical" S_2. A,C: high (default) fraction of induced catastrophes ($F_{ic} = 0.5$), B,D: Low fraction of induced catastrophes ($F_{ic} = 0.09$). $r_x = 0.1\ s^{-1}$. Error bars represent SEM with n=100 independent simulations per data point.

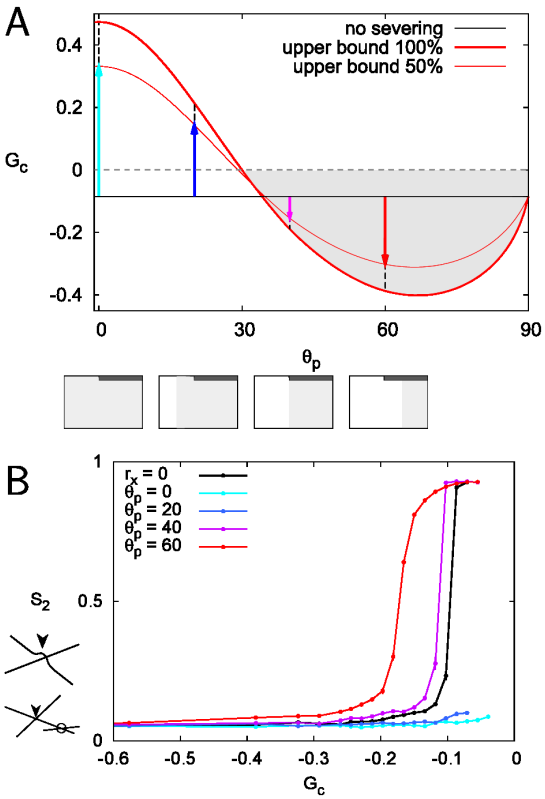

Fig. S5. Bundling normally protects nearly aligned MTs from crossover severing. *As figure 2BC, but with* $P_{cat} = 0.09$ *instead of the default* $P_{cat} = 0.5$. A: The theoretically estimated effect of protecting angles less than θ_p from severing: spontaneous alignment may occur in the gray area ($0 > G_c > G^*$). The thick red curves assume that severing at intersections is equally effective as direct induced catastrophes, which necessarily overestimates their effectiveness to some extent and thus provides an upper bound. The thin red curves show predictions for 50% effectiveness, illustrating the nonlinear approach towards the maximum. The cartoons at the bottom show the interaction functions used for C corresponding to the colored arrows: dark gray represents induced catastrophes, light gray represents crossovers that may be severed later and white crossovers that are protected from severing. B: The negative effect of crossing-only severing on alignment disappears if shallow angles (below $\theta_p = 20, 40, 60^\circ$) are protected from severing and turns into a positive effect for $\theta_p = 40^\circ$and 60°. Error bars represent SEM with n=100 independent simulations per data point.

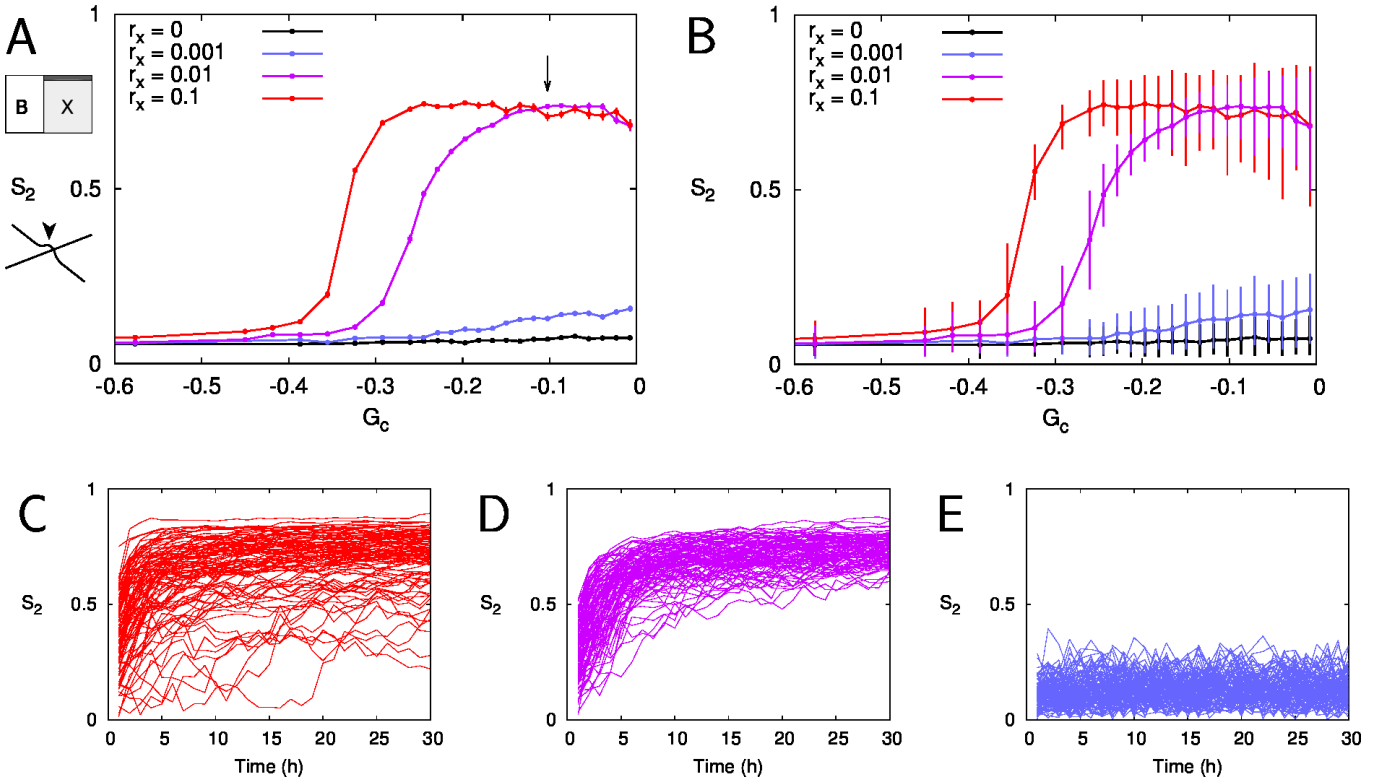

Fig. S6. Crossing-only severing is essential for alignment if induced catastrophes are rare ($P_{cat} = 0.09$). Bundling occurs for $\theta < 40°$. A,B: G_c, S_2 graphs for no severing (black), $r_x = 0.1\ s^{-1}$ (red), $r_x = 0.01\ s^{-1}$ (purple) and $r_x = 0.001\ s^{-1}$ (blue). All points are the average of 100 independent simulations. Error bars indicate SEM (A) or 10-90% intervals of the data (B). C,D,E: S_2-Time traces for all runs at $r_c = 0.0045\ s^{-1}$ ($G_c \approx -0.10$, see arrow in A). C: $r_x = 0.1\ s^{-1}$. D: $r_x = 0.01\ s^{-1}$. E: $r_x = 0.001\ s^{-1}$.

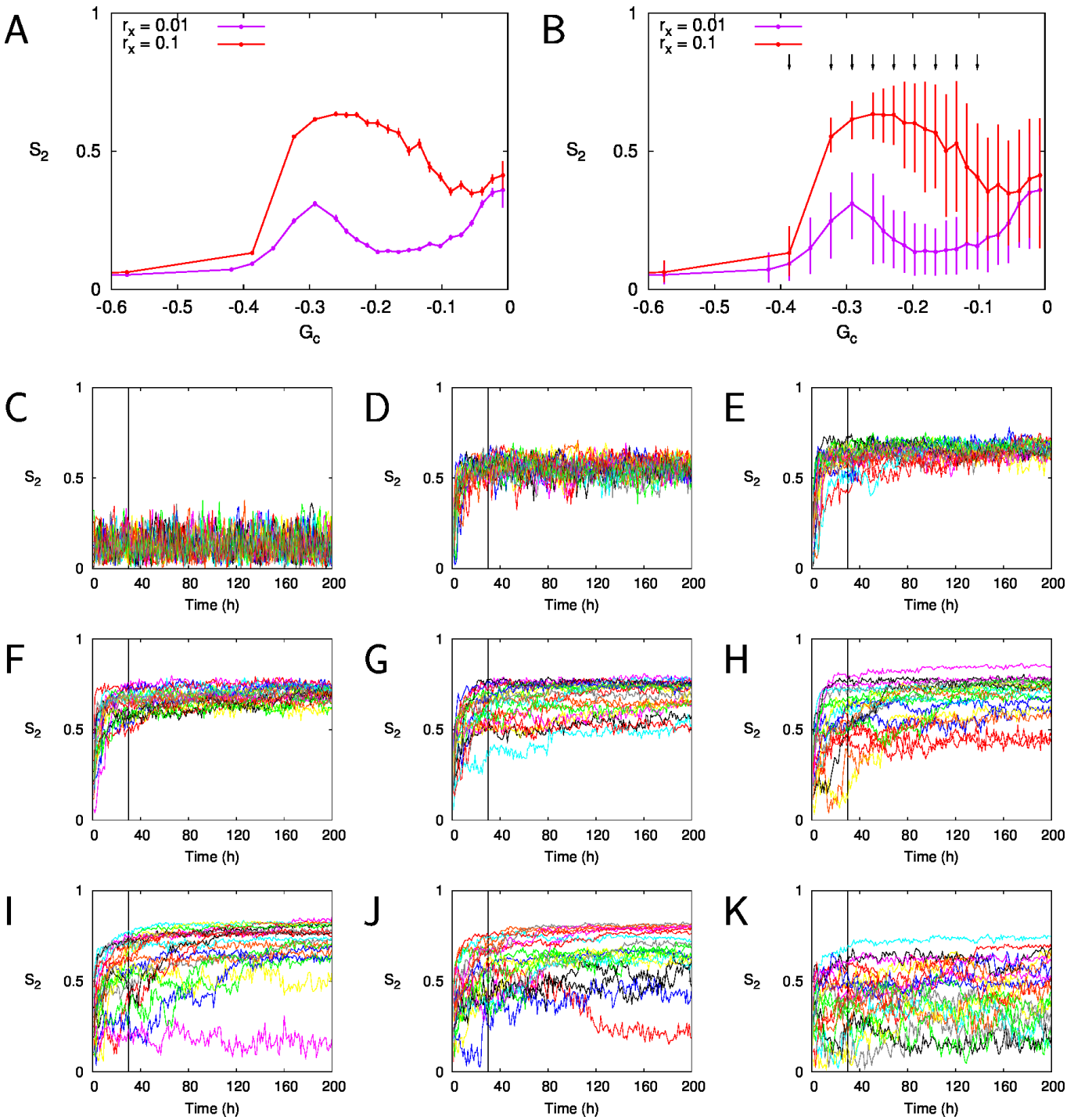

Fig. S7. Crossing-only severing can at best induce a moderate degree of alignment in absence of induced catastrophes ($P_{cat} = 0$), and is more efficient in combination with induced catastrophes A,B: Degree of global alignment S_2 after T=30h. n=100 individual simulations per point. Error bars indicate SEM (A) or 10-90% intervals of the data (B). C-K: Time traces for 200h for 20 independent simulations per parameter combination at the G_c-values indicated with arrows in B. The vertical black line indicates T=30h. All runs: $r_x = 0.1s^{-1}$. C: $r_c = 0.009s^{-1}$ D: $r_c = 0.008s^{-1}$ E: $r_c = 0.0075s^{-1}$ F: $r_c = 0.007s^{-1}$ G: $r_c = 0.0065s^{-1}$ H: $r_c = 0.006s^{-1}$ I: $r_c = 0.0055s^{-1}$ J: $r_c = 0.005s^{-1}$ K: $r_c = 0.0045s^{-1}$. See also fig. S8.

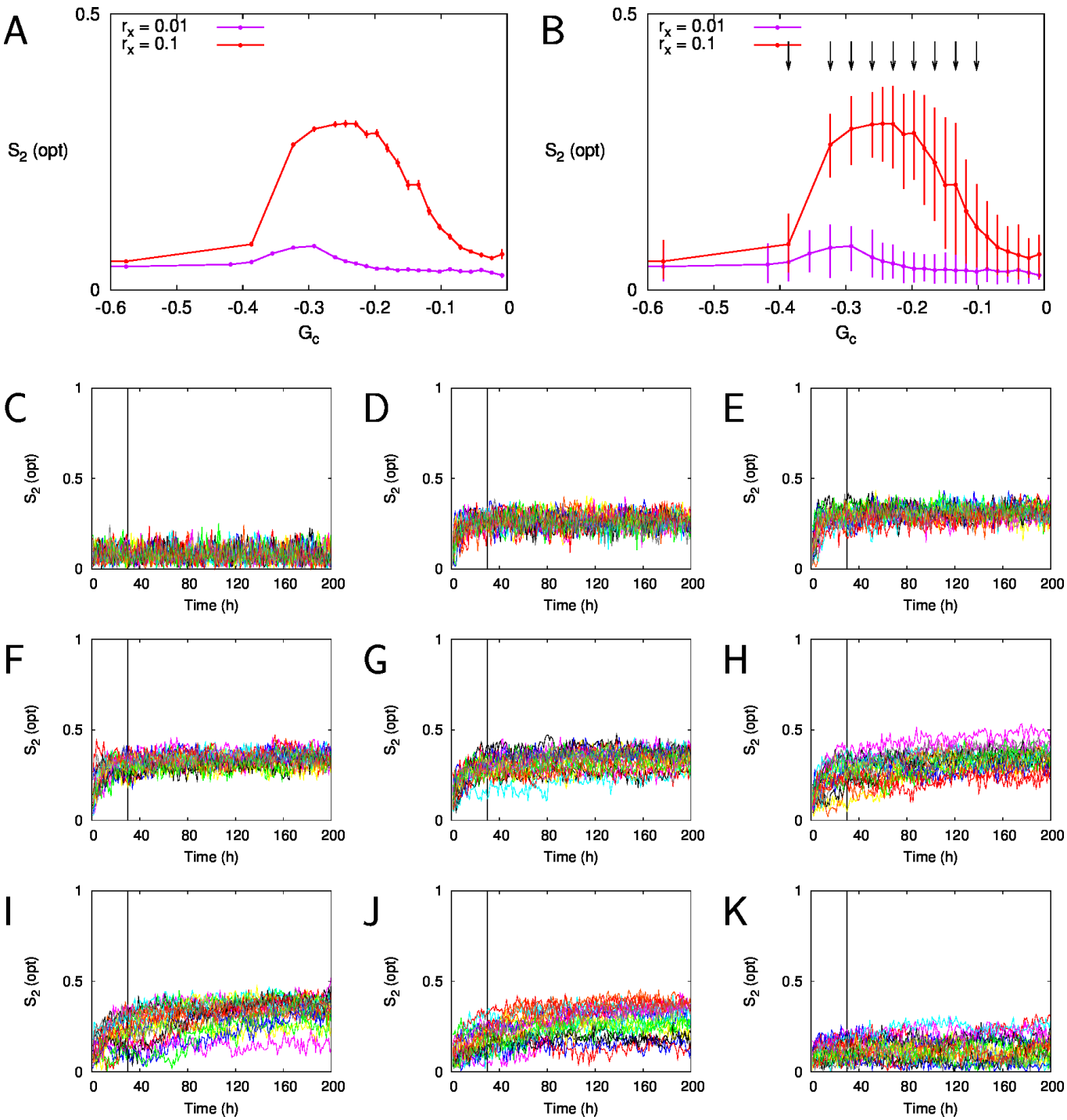

Fig. S8. *As figure S7 (no induced catastrophes; $P_{cat} = 0$), but with "optical" S_2: each bundled stretch of MTs is accounted as a singular MT part.* A,B: Degree of global alignment S_2(optical) after T=30h. n=100 individual simulations per point. Error bars indicate SEM (A) or 10-90% intervals of the data (B). C-K: Time traces for 200h for 20 independent simulations per parameter combination at the G_c-values indicated with arrows in B. The vertical black line indicates T=30h. All runs: $r_x = 0.1s^{-1}$. C: $r_c = 0.009s^{-1}$ D: $r_c = 0.008s^{-1}$ E: $r_c = 0.0075s^{-1}$ F: $r_c = 0.007s^{-1}$ G: $r_c = 0.0065s^{-1}$ H: $r_c = 0.006s^{-1}$ I: $r_c = 0.0055s^{-1}$ J: $r_c = 0.005s^{-1}$ K: $r_c = 0.0045s^{-1}$.

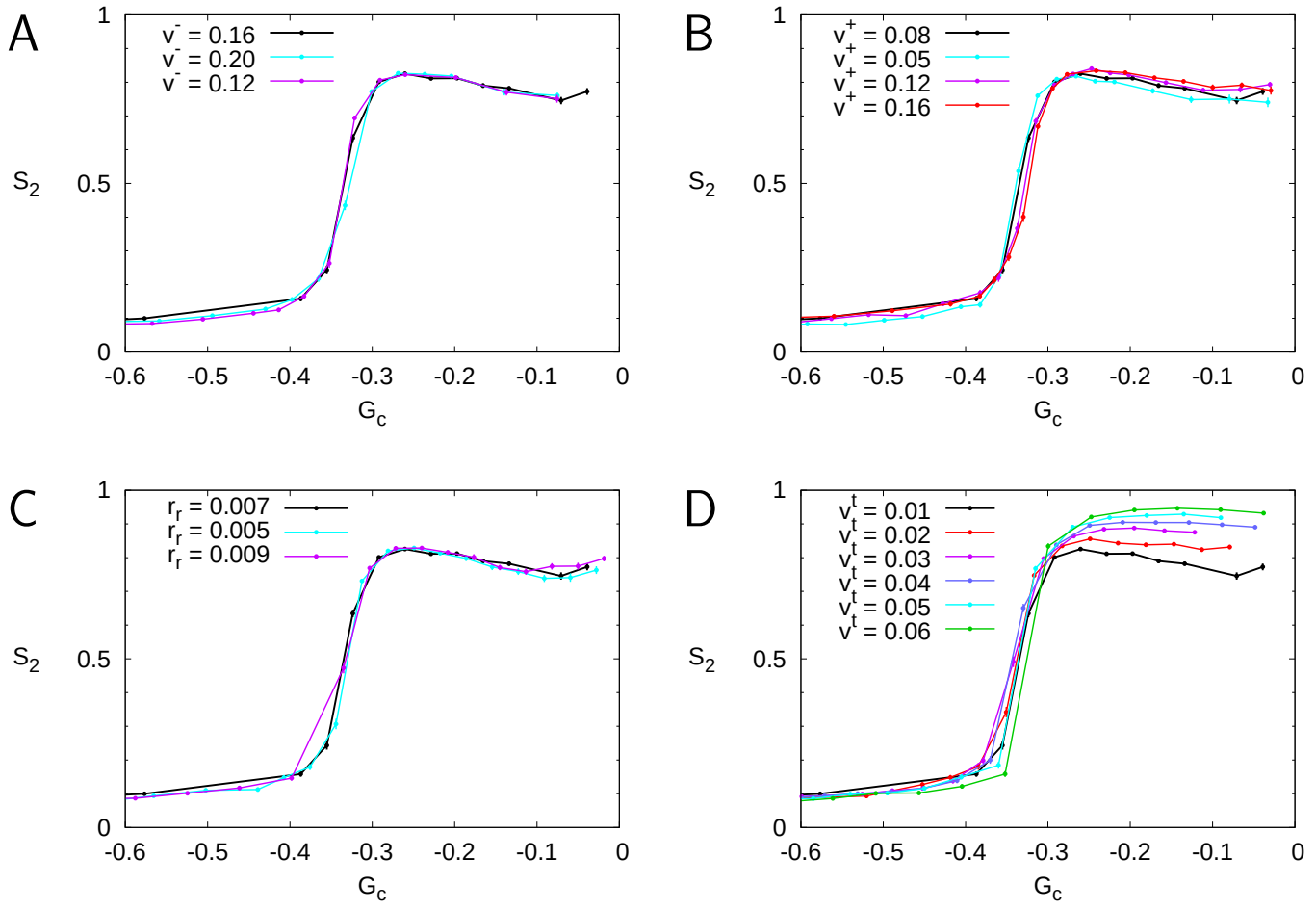

Fig. S9. Changes in MT stability do not affect the boundary (G^*) between disorder and alignment. Black lines indicate default parameter values, other values as indicated in the figures. A: varying v^- (unit: $\mu m/s$), B: varying v^+ (unit: $\mu m/s$), C: varying r_r (unit: s^{-1}), D: varying v^t (unit: $\mu m/s$). All figures: $r_x = 0.1/s$. Error bars indicate SEM of n=100 independent simulations per point. Data at T=30h.

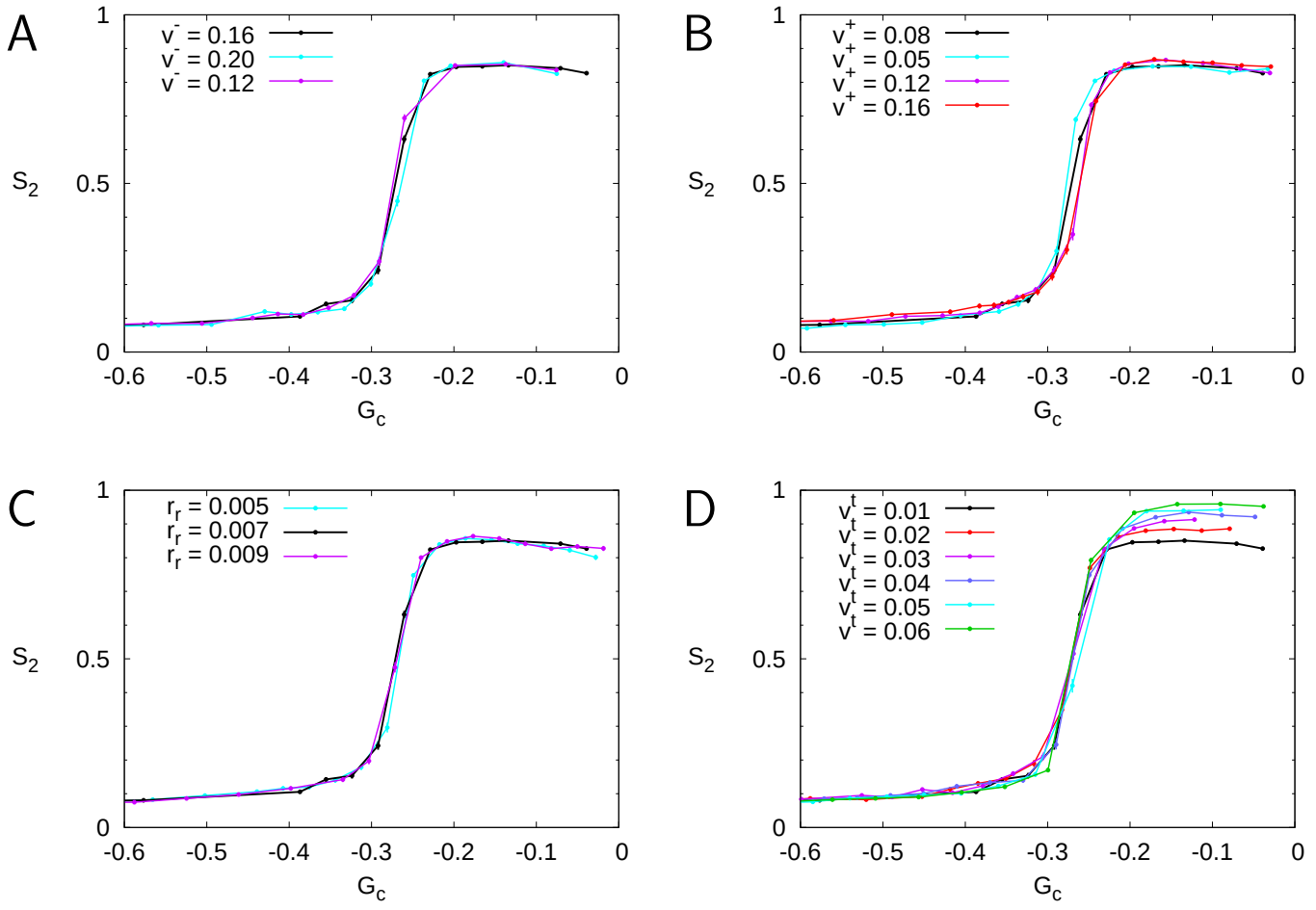

Fig. S10. Changes in MT stability do not affect the boundary (G^*) between disorder and alignment. *Similar to fig. S9, but with $r_x = 0.01/s$.* Black lines indicate default parameter values, other values as indicated in the figures. A: varying v^- (unit: $\mu m/s$), B: varying v^+ (unit: $\mu m/s$), C: varying r_r (unit: s^{-1}), D: varying v^t (unit: $\mu m/s$). All figures: $r_x = 0.01/s$. Error bars indicate SEM of n=100 independent simulations per point. Data at T=30h.

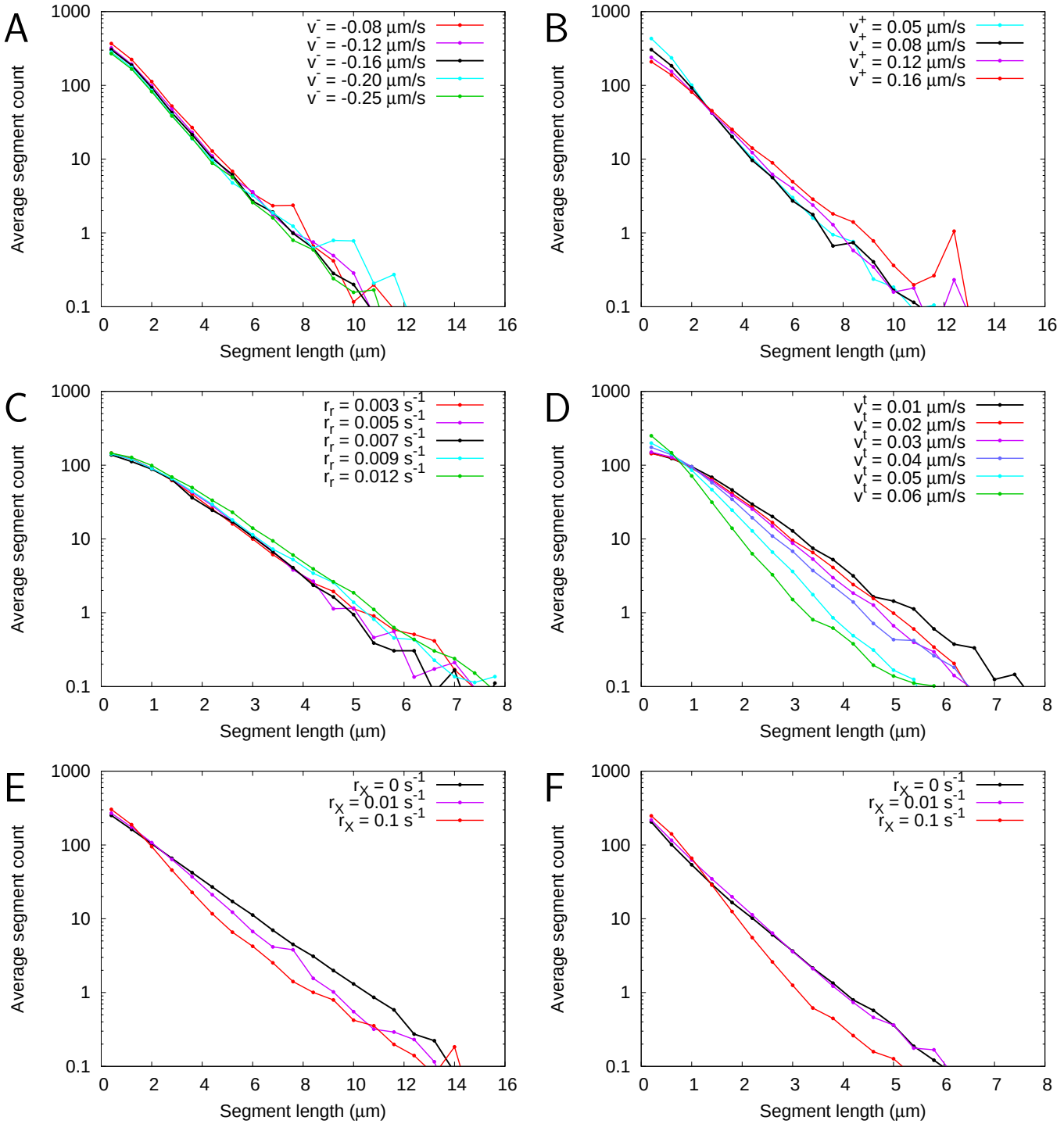

Fig. S11. Changes of length distributions at constant G_c depend on their effect on l_0, the average length of non-interacting MTs. Black lines indicate default parameter values, other values as indicated in the figures. A: varying v^-, B: varying v^+, C: varying r_r, D: varying v^t. E,F: Varying r_x. E: $v^t = 0.01\mu m/s$, F: $v^t = 0.04\mu m/s$. A-D: $r_x = 0.1/s$, n=100 independent simulations per point. Data at T=30h. For effects on l_0, see tables under text T5.

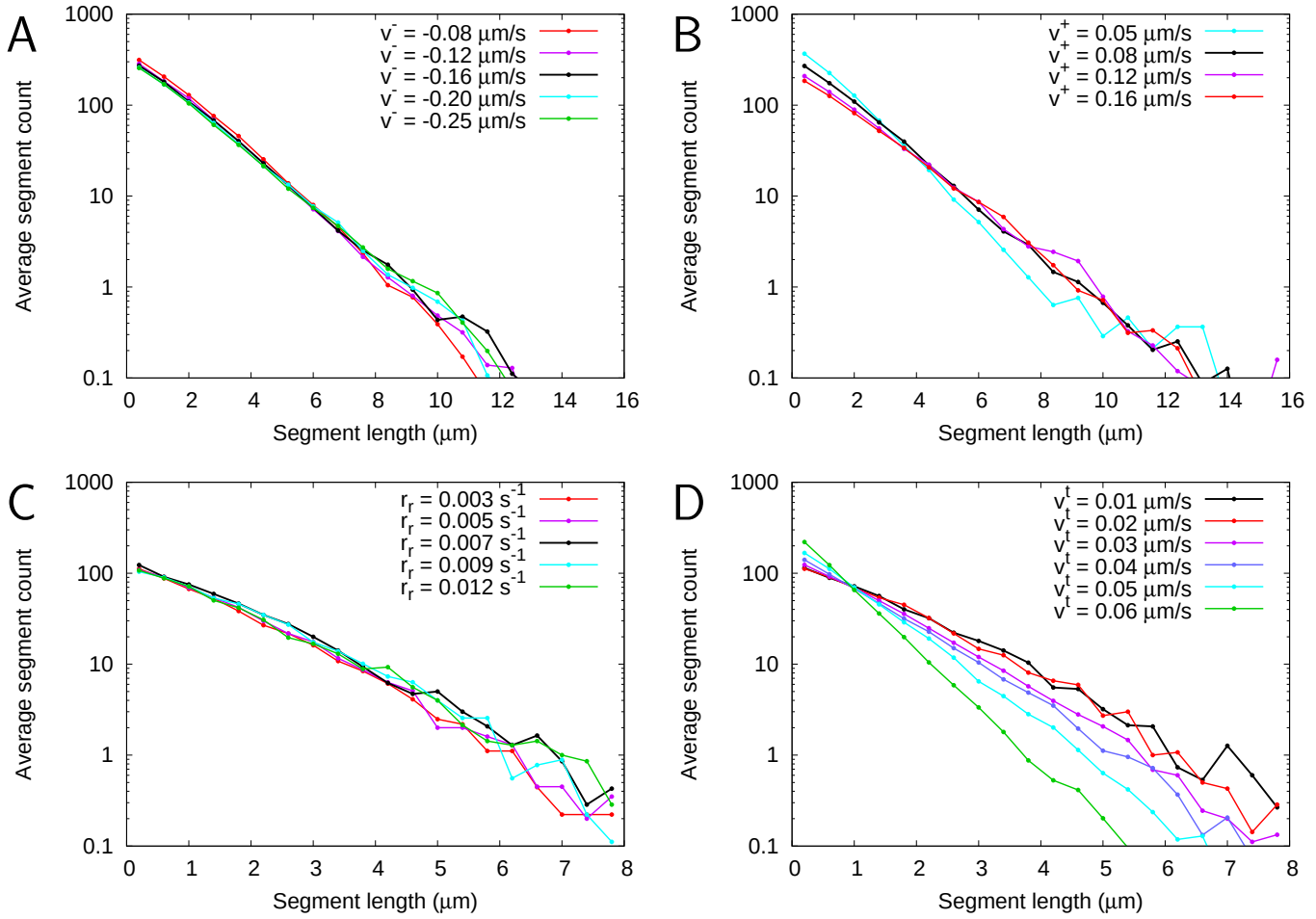

Fig. S12. Changes of length distributions at constant G_c depend on their effect on l_0, the average length of non-interacting MTs. *Similar to fig. S11, but with $r_x = 0.01/s$.* Black lines indicate default parameter values, other values as indicated in the figures. A: varying v^-, B: varying v^+, C: varying r_r, D: varying v^t. All figures: $r_x = 0.01/s$, n=100 independent simulations per point. Data at T=30h. For effects on l_0, see tables under text T5.

Supplementary Tables

Table S1. Overview of parameters.

Parameter	Default	Description
r_s	$0\ \mu\mathrm{m}^{-1}\,\mathrm{s}^{-1}$	Severing rate for random severing (per μm of MT length)
r_x	0 / 0.01 / 0.1 s^{-1}	Severing rate for crossover severing (per crossover)
–	crossing-only	Location of crossover severing: crossing-only or aselective (either side of the crossover)
θ_p	0°	Protected angle for crossover severing: no severing if the relative angle between MTs is $< \theta_p$. Only used in fig. 2
T	30h	Simulated time
v^+	$0.08\ \mu\mathrm{m}\,\mathrm{s}^{-1}$	Growth speed
v^-	$0.16\ \mu\mathrm{m}\,\mathrm{s}^{-1}$	Shrinkage speed
v^t	$0.01\ \mu\mathrm{ms}^{-1}$	Treadmilling speed
r_r	$0.007\ \mathrm{s}^{-1}$	Rescue rate
r_c	variable: 0.003 – $0.010\ \mathrm{s}^{-1}$; default: $0.0045\mathrm{s}^{-1}$	Spontaneous catastrophe rate
r_n	$0.001\ \mathrm{s}^{-1}\,\mu\mathrm{m}^{-2}$	Nucleation rate
θ^*	40°	Maximum bundling angle
P_{cat}	0.5	Induced catastrophe probability (for $\theta > \theta^*$)
$W \times H$	$80 \times 80\ \mu\mathrm{m}$	System size (periodic boundaries)
F_t	1	Fraction of crossover severing events in which the crossing MT (bundle) was selected for severing. Only used explicitly in fig. S4. $F_t = 1$ is the same as crossing-only severing, $F_t = 0.5$ is the same as aselective crossover severing.

Table S2. Short MT abundances based on maximum histogram lengths of 16 μm (top) or 8 μm (bottom).

				$S_2\pm$ SEM			Fraction of MTs shorter than: 0.8 μm	1.6 μm	0.8 μm	1.6 μm	0.8 μm	1.6 μm
		r_c (s^{-1})	l_0 (μm)	$r_x = 0.1$/s	$r_x = 0.01$/s	$r_x = 0$/s	$r_x = 0.1$/s		$r_x = 0.01$/s		$r_x = 0$/s	
v^t	0.01	0.00481	36.4	0.75 ± 0.012	0.86 ± 0.004	0.90 ± 0.003	0.44	0.72	0.38	0.63	0.36	0.59
	0.02	0.00413	33.4	0.84 ± 0.005	0.88 ± 0.004	0.92 ± 0.003	0.46	0.74	0.38	0.63	0.38	0.62
	0.03	0.00350	30.2	0.87 ± 0.005	0.92 ± 0.004	0.94 ± 0.003	0.49	0.77	0.42	0.67	0.42	0.66
	0.04	0.00291	26.4	0.91 ± 0.004	0.93 ± 0.004	0.95 ± 0.003	0.54	0.81	0.47	0.72	0.47	0.71
	0.05	0.00235	22.2	0.92 ± 0.004	0.95 ± 0.003	0.96 ± 0.003	0.61	0.86	0.55	0.80	0.56	0.78
	0.06	0.00180	17.2	0.95 ± 0.003	0.96 ± 0.003	0.97 ± 0.003	0.72	0.92	0.66	0.87	0.66	0.86
v^-	0.08	0.00752	33.8	0.77 ± 0.010	0.85 ± 0.005	–	0.45	0.72	0.38	0.63	–	–
	0.12	0.00574	35.5	0.77 ± 0.010	0.84 ± 0.005	–	0.45	0.72	0.39	0.63	–	–
	0.16	0.00480	36.5	0.77 ± 0.010	0.85 ± 0.005	–	0.45	0.72	0.38	0.63	–	–
	0.20	0.00421	37.2	0.76 ± 0.010	0.84 ± 0.004	–	0.45	0.72	0.38	0.63	–	–
	0.25	0.00374	37.8	0.76 ± 0.009	0.85 ± 0.005	–	0.45	0.72	0.38	0.63	–	–
v^+	0.05	0.00295	30.7	0.75 ± 0.012	0.84 ± 0.006	–	0.50	0.78	0.42	0.68	–	–
	0.08	0.00480	36.5	0.76 ± 0.011	0.84 ± 0.006	–	0.45	0.73	0.38	0.63	–	–
	0.12	0.00722	40.9	0.78 ± 0.008	0.86 ± 0.004	–	0.42	0.68	0.36	0.60	–	–
	0.16	0.00960	43.7	0.79 ± 0.007	0.86 ± 0.005	–	0.40	0.66	0.35	0.58	–	–
r_r	0.003	0.00315	36.5	0.75 ± 0.011	0.83 ± 0.005	–	0.46	0.73	0.40	0.64	–	–
	0.005	0.00398	36.5	0.77 ± 0.008	0.84 ± 0.006	–	0.45	0.73	0.39	0.64	–	–
	0.007	0.00480	36.5	0.77 ± 0.010	0.85 ± 0.004	–	0.44	0.71	0.38	0.63	–	–
	0.009	0.00562	36.5	0.77 ± 0.008	0.85 ± 0.005	–	0.44	0.72	0.37	0.62	–	–
	0.012	0.00686	36.5	0.78 ± 0.010	0.85 ± 0.005	–	0.43	0.71	0.37	0.61	–	–

				$S_2\pm$ SEM			Fraction of MTs shorter than: 0.8 μm	1.6 μm	0.8 μm	1.6 μm	0.8 μm	1.6 μm
		r_c (s^{-1})	l_0 (μm)	$r_x = 0.1$/s	$r_x = 0.01$/s	$r_x = 0$/s	$r_x = 0.1$/s		$r_x = 0.01$/s		$r_x = 0$/s	
v^t	0.01	0.00481	36.4	0.75 ± 0.012	0.86 ± 0.004	0.90 ± 0.003	0.48	0.77	0.42	0.68	0.41	0.66
	0.02	0.00413	33.4	0.84 ± 0.005	0.88 ± 0.004	0.92 ± 0.003	0.49	0.78	0.42	0.68	0.47	0.71
	0.03	0.00350	30.2	0.87 ± 0.005	0.92 ± 0.004	0.94 ± 0.003	0.52	0.81	0.46	0.73	0.50	0.75
	0.04	0.00291	26.4	0.91 ± 0.004	0.93 ± 0.004	0.95 ± 0.003	0.58	0.86	0.52	0.77	0.56	0.80
	0.05	0.00235	22.2	0.92 ± 0.004	0.95 ± 0.003	0.96 ± 0.003	0.65	0.90	0.59	0.83	0.64	0.86
	0.06	0.00180	17.2	0.95 ± 0.003	0.96 ± 0.003	0.97 ± 0.003	0.77	0.95	0.70	0.90	0.71	0.90
v^-	0.08	0.00752	33.8	0.77 ± 0.010	0.85 ± 0.005	–	0.49	0.78	0.42	0.68	–	–
	0.12	0.00574	35.5	0.77 ± 0.010	0.84 ± 0.005	–	0.49	0.78	0.41	0.67	–	–
	0.16	0.00480	36.5	0.77 ± 0.010	0.85 ± 0.005	–	0.49	0.77	0.42	0.68	–	–
	0.20	0.00421	37.2	0.76 ± 0.010	0.84 ± 0.004	–	0.48	0.77	0.41	0.67	–	–
	0.25	0.00374	37.8	0.76 ± 0.009	0.85 ± 0.005	–	0.49	0.78	0.41	0.67	–	–
v^+	0.05	0.00295	30.7	0.75 ± 0.012	0.84 ± 0.006	–	–	–	–	–	–	–
	0.08	0.00480	36.5	0.76 ± 0.011	0.84 ± 0.006	–	–	–	–	–	–	–
	0.12	0.00722	40.9	0.78 ± 0.008	0.86 ± 0.004	–	–	–	–	–	–	–
	0.16	0.00960	43.7	0.79 ± 0.007	0.86 ± 0.005	–	–	–	–	–	–	–
r_r	0.003	0.00315	36.5	0.75 ± 0.011	0.83 ± 0.005	–	0.50	0.79	0.43	0.69	–	–
	0.005	0.00398	36.5	0.77 ± 0.008	0.84 ± 0.006	–	0.49	0.78	0.42	0.68	–	–
	0.007	0.00480	36.5	0.77 ± 0.010	0.85 ± 0.004	–	0.48	0.78	0.41	0.67	–	–
	0.009	0.00562	36.5	0.77 ± 0.008	0.85 ± 0.005	–	0.48	0.77	0.40	0.66	–	–
	0.012	0.00686	36.5	0.78 ± 0.010	0.85 ± 0.005	–	0.47	0.76	0.40	0.66	–	–

References

1. Lindeboom JJ, et al. (2013) Cortical microtubule arrays are initiated from a nonrandom prepattern driven by atypical microtubule initiation. *Plant Physiol* 161(3):1189–1201.
2. Tindemans SH, Deinum EE, Lindeboom JJ, Mulder B (2014) Efficient event-driven simulations shed new light on microtubule organisation in the plant cortical array. *Frontiers in Physics* 2(19):9.
3. Dogterom M, Leibler S (1993) Physical aspects of the growth and regulation of microtubule structures. *Physical Review Letters* 70(9):1347–1350.
4. Hawkins RJ, Tindemans SH, Mulder BM (2010) Model for the orientational ordering of the plant microtubule cortical array. *Physical review. E, Statistical, nonlinear, and soft matter physics* 82(1 Pt 1):011911.
5. Tindemans SH, Mulder BM (2010) Microtubule length distributions in the presence of protein-induced severing. *Phys Rev E Stat Nonlin Soft Matter Phys* 81(3 Pt 1):031910.
6. Deinum EE (2013) Ph.D. thesis.